CHAPTER 1

INTRODUCTION

There is a growing interest in the automatic analysis of images acquired in scattering media. A main objective in such analysis is improvement of visibility and recovery of colors, as if imaging is done in clear conditions. Computer vision and human vision can then capitalize on such improved images for various applications, such as long range surveillance, targets detection and recognition, navigation and photography. Haze along with fog and clouds are limiting factors for visual range in the atmosphere and heavily reduce contrast in scenes. E. Namer and Y. Y. Schechner, two of the current experts in this field described the need for dehazing algorithms as "There is a growing interest in the automatic analysis of images acquired in scattering media. A main objective in such analysis is improvement of visibility and recovery of colors, as if imaging is done in clear conditions. Computer vision and human vision can then capitalize on such improved images for various applications, such as long range surveillance." [1]. Also the haze-free image is more pleasuring visually. Second, most computer vision algorithms, from low-level image analysis to high-level object recognition, usually assume that the input image (after radiometric calibration) is the scene radiance. The performance of computer vision algorithms (*e.g.*, feature detection, filtering, and photometric analysis) will inevitably suffer from the biased, low-contrast scene radiance. Last, the haze removal can produce depth information and benefit many vision algorithms and advanced image editing. Haze or fog acts as a useful depth clue for scene understanding.

The image with bad haze can be put to good use. [2]. The need for image enhancement originates from the fact that the atmosphere is never free of particles. With pure air, the visual range has been found to be ranging between 277km to 348km, without considering the curvature of the earth surface. However, real visual ranges are very less than the theoretical value. The international visibility code for meteorological range rates visibilities between under 50m up to over 50km for exceptionally clear air. These codes have been found to reflect a convenient scale for visual ranges in the daily work of meteorologists. For the exact codes please refer to table 1.1, the scattering coefficient β_{sc} is an important parameter in visual range and will be dealt with in a separate section in this thesis (chapter 2).

Code no.	Weather Condition	Meteorological Range, R_m	Scattering coefficient, $\beta_{sc}(km^{-1})$
0	Dense fog	$\leq$ 50m	>78.2
1	Thick fog	50m - 200m	78.2 - 19.6
2	Moderate fog	200m - 500m	19.6 - 7.82
3	Light fog	500m - 1000m	7.82 - 3.91
4	Thin fog	1km - 2km	3.91 - 1.96
5	Haze	2km - 4km	1.96 - 0.954
6	Light haze	4km - 10km	0.954 - 0.391
7	Clear	10km - 20km	0.391 - 0.196
8	Very clear	20km - 50km	0.196 - 0.078
9	Exceptionally clear	>50km	0.078
-	Pure air	277km	0.0141

Table 1.1.: International Visibility Code with Meteorological Range

For many centuries optical effects in the atmosphere have been studied. Early motivations have been to understand the colour shifts of distant objects and all optical effects that can be seen by observing nature through the atmosphere like the blueness of the sky or the red of the dawning sun. The first work, that is still to be deemed as outstanding today, is the work of Lord Rayleigh who examined light scattering in 1871 and in the following years(e.g. [3]). With the development of airplanes a new motivation was incepted and research for "optics of the atmosphere" began to increase. At the beginning of the 19th century, scientists like Mie and Koschmieder developed theories that are still used in today's work in meteorology and computer vision. Mie (1908) expanded the theory of Rayleigh by examining larger particles such as haze aerosols, that have a great influence in scattering and extinction of light in the atmosphere. Koschmieder (1924) took the essential step from the scattering theories and developed an holistic theory for horizontal visual ranges through the atmosphere, which describes the visibility of a distant object, based on illumination, several environmental factors and the composition of the air in the scene of interest. Much of the research was driven by the first and second world war. Visibility range in various altitudes of the atmosphere, as well as the development of chemical warfare methods that were intended to reduce visibility for hostile airplane pilots were the subjects of meteorological research at that time. Nevertheless, the work from that time is the basis for what we know about optics of the atmosphere today.

With the help of these theories, one can explain the effects that haze has on the visibility of a scene and eventually of an image taken of that scene. Moreover, this knowledge can be

used to improve visibility for the human eye and develop techniques for removing haze. It is possible to improve the visibility in terms of range, colour verisimilitude and feature separation in digital images. Herein the term "dehazing" means to produce an image of a scene that does not contain haze effects although the source of that image originally comprised haze, for an example please refer to figure 1.1.

Figure 1.1.: Images show the hazy input image and the dehazed result using the algorithm of Fattal [4]

"Defogging" will also be subject to this work since the effects of haze and fog are to some degree similar and the transition between the two phenomena is gradual. Defogging and dehazing can greatly improve the visibility for the human eye and allow the observer to get a much higher situational awareness. Such visibility improvements may lead to a smoother and faster work flow in areas where operators need to observe a wide area under every possible weather conditions at day and night. Such as an air traffic controller at an airfield, possibly at a tower or a remote position, respectively. In recent years much work was done on dehazing algorithms utilising different kinds of computer hardware. The main goal of this thesis is to develop a dehazing method that is capable of enhancing image output and removing block effect and halo effect.

CHAPTER 2

VISION THROUGH THE ATMOSPHERE

From very past times our principal knowledge of the physical world has been derived from the basic act of seeing [5].

Fact is, that often the only information we have of a distant object is the visual information which travelled through and was altered by the atmosphere. We heavily rely on that information, because we use it to detect, recognise, identify and position objects. We will first give a brief overview of the basics of the atmosphere in terms of particle, followed by a review of light scattering. In the last section we will discuss very important "Theorie der Horizontalen Sichtweite" of Koschmieder.

2.1 Atmosphere Basics

As light travels through a medium, it will most likely get altered due to interactions with the particles of that medium if the travel distance through that medium is sufficiently long. Reflections, scattering or absorption may happen depending on various factors of the medium. Due to these effects, it is plausible to conclude that light can't travel endlessly through a medium and especially not undistorted. To understand how exactly the atmosphere alters incident light, one must have a closer look at the composition of air and the atmosphere. This section will give a broad overview of the composition of the atmosphere and the origination of particles. The author will conclude the section with an observation of special atmospheric conditions such as fog and clouds.

2.1.1 Optical Concepts in Atmospheric Vision

This subsection shall cover the basic optical concepts that will be used throughout this thesis. The term visibility in this context is synonymous to visual range, which is a measurement being very subjective and varying from person to person. Visual range is defined as the range to where a reference object is just discriminable from the background, or in other words "the distance, under daylight conditions, at which the apparent contrast between a specified type of target and its background (horizon sky) becomes just equal to the threshold contrast of an observer". The visual range therefore depends on the observer

(due to the threshold contrast), the size and constitution of the reference object and the background light. The formula for visual range assuming a standard reference object R_v is:

$$R_V = \frac{1}{\beta sc} ln \frac{C}{\epsilon} \tag{2.1}$$

Where C is the contrast of the target against the background, ϵ is the threshold contrast of the observer (a basic value can be obtained for example from the Tiffany Foundation data), and β_{sc} is the scattering coefficient. The thesis will discuss the scattering coefficient later in detail in the scattering section. Due to the threshold contrast ϵ, the photographic range is always greater than the visual range, since the photographic range uses the same formula as the R_v but with a minimal ϵ. Humans can only distinct two objects when the contrast is high enough, with photographs however, this contrast can be modified and visibility improved. These subjective factors have been eliminated in the meteorological range R_m. The standardised reference object is a black body radiator that is large enough for the scene and ϵ= 0.02, which is not far from the actual threshold contrast of a human eye in daylight conditions. Since the target is black, its inherent contrast against the sky is unity, and equation 2.1 becomes

$$R_m = \frac{1}{\beta sc} ln \frac{C}{0.02} = \frac{3.912}{\beta sc} \tag{2.2}$$

which is, although empiric too, far more convenient. The meteorological range is also called standard visibility or standard visual range. Typical scattering coefficients can be obtained from table 1.1 on page 2. In aviation meteorology, the runway visual range (RVR) is often used, which defines the distance over which a pilot of an aircraft standing on the centerline of a runway can see the runway surface markings defining the runway or identifying its center line. This is a special case of the visual range R_v.

2.1.2 Relative Humidity

As we have described, particle sizes of hygroscopic nuclei are much influenced by the relative humidity. For better understanding, this subsection will describe the concept of relative humidity in more detail since it will be used in later sections as well.

The humidity of the air denotes the proportion of vaporised water in the air compound. Hence liquid or solid forms of water are not measured for air humidity. Humidity is an important parameter for meteorological and technical processes, for this purpose however

it is an important factor for visibility through haze, fog and clouds, respectively. At a certain temperature and pressure, only so much vaporised water can be contained by a unit volume of air. The most common measure for humidity is the relative humidity that is given in per cent. It denotes the proportion of the current amount of water vapour to the maximum possible amount of water vapour at the same air pressure and temperature. The formula for relative humidity therefore is:

$$relative\ humidity[\%] = \frac{current\ absolute\ humidity[g/m3]}{maximal\ absolute\ humidity[g/m3]}\ x100 \tag{2.3}$$

Although there is no compulsory symbol, relative humidity is often written as the Greek letter ϕ, thus the equation can be simply written as:

$$\phi = \frac{s}{S}\ x100 \tag{2.4}$$

With *s* the specific humidity and *S* the saturation humidity. As stated earlier, hygroscopic nuclei grow in size with relative humidity, since bigger particles are able to scatter light better than small particles, this results in a dependency of visual range to relative humidity. Figure 2.1 shows this correlation. The curve is an average of many observations at the some airport, a region that is very rich of nuclei.

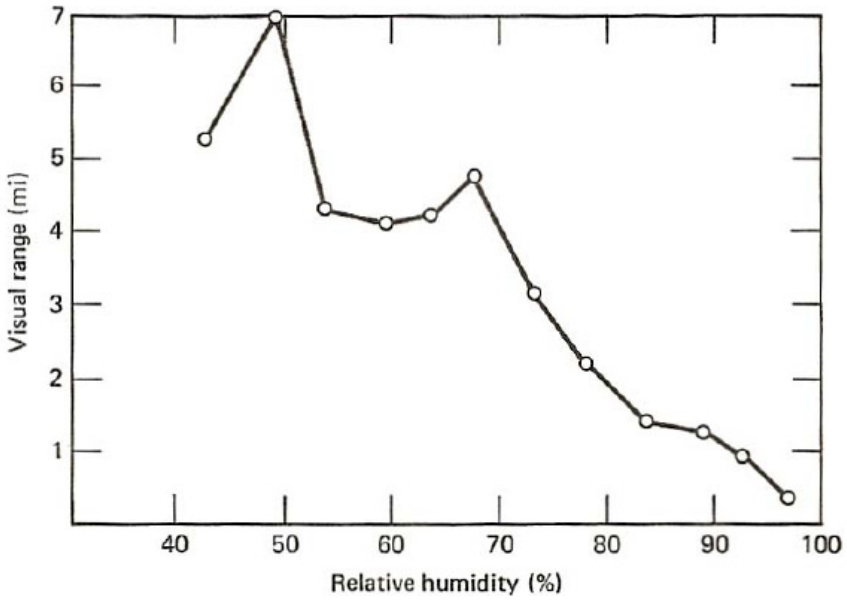

Figure 2.1.: Visual range as a function of relative humidity at some airport.

2.1.3 Fog, Clouds and Smoke

Along with haze and dust, the latter usually implying that the air is dry, there are other hygroscopic and non hygroscopic objects which will be the topic of this subsection. The distinction between the humid phenomena can be made through the droplet size and concentration as it is shown in table 1.1 on page 2. As a rule of thumb, the higher the concentration and the bigger the particles are, the more they will scatter light, hence the visual range will drop. Although water absorbs certain wavelengths, it does not absorb all light, however some particles, especially black smoke particles are able to absorb visible light independent from wavelength. This will of course result in a strongly decreased visual range. These particles would need further classification. It is also noteworthy that clouds are not the same as fog, the visual effects are of different magnitude as are the constituents in terms of size, size distribution and number. To visualise the droplet size, one should have a look at figure 2.2, it shows the differences in particle sizes of cloud, fog and haze drawn to the same scale.

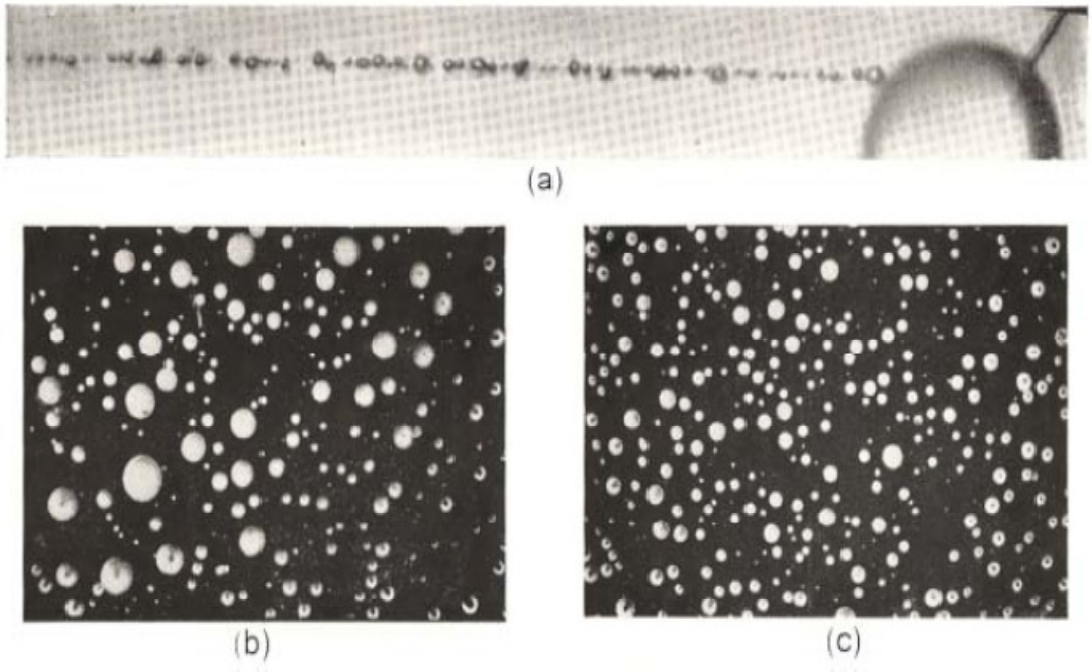

Figure 2.2.: Photographs of Cloud, Fog and Haze Droplets. (a) shows the photomicrograph of haze particles, (b) shows a photomicrograph of typical fog particles, (c) shows a photomicrograph of typical cloud particles.

These photographs however only show certain types of clouds and fogs, the fog shown in figure 2.2 is a coastal fog with larger droplets than the cloud and also a larger range of radii. Clouds also are not always of the same type, since they may have different origins and altitudes. Common mean radii of clouds depend on their type: Nimbostratus(10μm), Stratocumulus(8μm), Cumulus(5μm) and Stratus(4μm). However all these particles and cloud types, even rain could be described by the power-law size distribution function, described in the earlier subsection. This shall just show the large variety of particles in the air and their constitution and origin, respectively. It is therefore a complex problem to find a dehazing algorithm that can handle all kinds of haze, clouds, fog and smoke, respectively. The formation of clouds and fog however are not topic of this thesis. At this point, the reader should have enough basic knowledge to understand the upcoming core principles such as light scattering and the "Theorie der horizontalen Sichtweite" after Koschmieder. The author wishes to address only one more topic before the thesis will carry on with the core principles.

As it was addressed by Middleton in 1952 already, there is a myth of a diffuse boundary of fog and smoke. A common belief is that fog inherits the ability to distort shapes/outlines. Such that, for example the outline of a person seen through a wall of fog, is horizontally or otherwise distorted and that the actual outline cannot be seen. There is no scientific data that shows this phenomenon. All photographs that show objects through thick fog either show clear outlines of that object or no object due to light extinction. It is more a stylistic device of painters than a real world effect. This can also be shown by light beams, for example that of a flashlight seen in fog or smoke, although the light appears weaker along the path as it travels through the medium, the boundaries of the cone or beam are not diffuse but indeed sharp. This is a fortunate characteristic and therefore does not need further regard from the dehazing algorithm.

2.2 Light Scattering

Light scattering is the most important phenomenon to this subject. It describes the interaction between a (haze) particle and a photon. This section will deal with light scattering in detail, initially from a general perspective but then in subsequent sections with respect to Rayleigh scattering and Mie scattering. But first, a motivation for scattering research is given.

2.2.1 Motivation

In a common scenario where air molecules are in a concentration of N_L = 2.687 × 1019cm^{-3} (Loschmidt's number), the average spacing available to each molecule is 1/N_L cm3. Hence the average spacing between air molecule centres is

$$S = \sqrt[3]{1/N_L} \approx 3.3 \times 10^{-7} cm \approx 33Å \tag{2.5}$$

which is about 9 times the diameter. The mean free path l, usually used to express the average distance a molecule travels between collisions is given by

$$l = \frac{1}{\sqrt{2}\pi d^2 N_L} \tag{2.6}$$

this adds up to about 600Å when using the effective collision area of $A = \pi d^2$ with the diameter for air molecules. However to show that a photon will in most cases collide with an air molecule or haze particle in distances common for visual ranges, one can use the effective collision area of a photon with an air molecule instead. A photon, not having a radius, causes the effective collision area to be just $A = \pi r^2$. With r the radius of an air molecule, one will get for the mean free path:

$$l = \frac{1}{\sqrt{2}\pi d^2 N_L} \approx 2.4x10^{-7} cm \approx 2400Å \tag{2.6}$$

This shows that the distance travelled by a photon through air is, although considerably longer than that of an air molecule, extremely small compared to visual ranges. This should be motivation enough to take a closer look at the scattering process itself.

2.2.2 General Considerations of Light Scattering

As a rule of thumb, it can be said that, the larger a particle is, the better it scatters light. This phenomenon is illustrated by figure 2.3, the figures show the scattering pattern of a light beam scattered by 3 different sizes of particles (a) shows the symmetric scattering pattern of a particle smaller than one-tenth of the wavelength of the incident light beam. (b) and (c) show the scattering patterns of larger particles, note that the complexity of the pattern grows with the particle size. The similarity of all scattering patterns of particles

larger than one-tenth of the wavelength of the light is that most photons are scattered in forward direction, this effect is increased also with particle size.

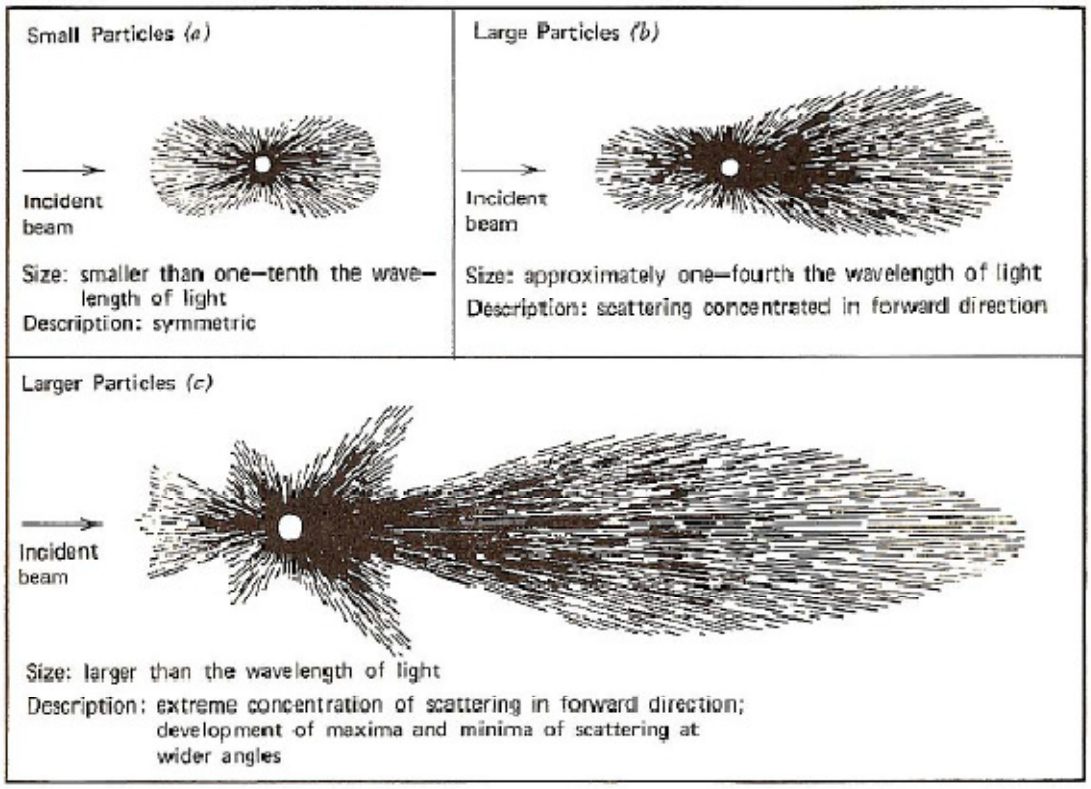

Figure 2.3.: Angular patterns of scattered intensity from particles of three sizes. (a) Small particles, (b) large particles, (c) larger particles.

Because of the large magnitude of visual ranges compared to that of the mean free path, a photon can get scattered by more than one particle along the way between the object and the eye of the observer, this is called multi scattering or rescattering, respectively. However, throughout this section single scattering is considered first in order to describe the basic mechanisms of scattering. There are two main theories that explain light scattering, they are named after their originators, the Mie scattering and the Rayleigh scattering. They both describe the phenomenon of light scattering, however assuming different sizes of particles. Whereas the Mie theory can be used to describe scattering by larger particles such as haze, Rayleigh scattering can be used to explain, among other things, the blueness of the sky due to air molecule scattering. Scattering is an important effect of the atmosphere and all particles contained within, it delimits the visual range. It

was attempted to quantify this by introducing the scattering coefficient β. The scattering coefficient is a part of the extinction coefficient σ:

$$\sigma = \beta + k \tag{2.7}$$

with k being the absorption coefficient. For now however, consider an absorption free atmosphere, meaning the total flux of the incident beam is equal to the total flux of the scattered light in all directions. The scattering function $\beta(\phi)$, which dependents on the observed angle in relation to the incident beam, denotes how much of the incident beam will get scattered in the direction with the angle ϕ, the scattering function is contained in the equation:

$$I(\phi) = Eds \cdot \beta(\phi) \tag{2.8}$$

With $I(\phi)$, the light intensity produced by the incident beam and E, the illuminance at ds. In the absence of absorption it is:

$$\int_0^{4\pi} I(\phi) d\omega \ = E\, ds \tag{2.9}$$

Or,

$$2\pi \int_0^{\pi} E\ ds\ \ \beta(\phi)\, sin\, \phi d\phi = E\, ds \tag{2.10}$$

And therefore

$$2\pi \int_0^{\pi}\ \ \beta(\phi)\, sin\, \phi d\phi = 1 \tag{2.11}$$

Likewise the volume scattering function $\beta'(\phi)$ is:

$$2\pi \int_0^{\pi}\ \ \beta'(\phi)\, sin\, \phi d\phi = \beta \tag{2.12}$$

This relation is useful when the actual scattering material is unknown. The scattering coefficient will be used in the following subsections for Mie and Rayleigh scattering. Actual scattering coefficients for various visual ranges can be found in table 1.1 on page 2. It will now be shown how the scattering actually works, first for very small particles (Rayleigh scattering) and then for larger particles (Mie scattering).

2.2.3 Rayleigh Scattering

Rayleigh Scattering is named after the British physicist Lord Rayleigh and describes the elastic scattering of light. The light is considered as an electromagnetic wave scattered by particles much smaller than the wavelength of the radiation. The theory holds for transparent media of all aggregate states. The ratio α, which describes the relation between the wavelength of the incident light and the particle radius, can be used to delimit the transition between Rayleigh scattering and Mie scattering. "The joint importance of wavelength and particle size may be appreciated from the fact that these two parameters determine the distribution of phase over the particle." [5]

$$\alpha = \frac{2\pi r}{\lambda} \tag{2.13}$$

Rayleigh scattering can be defined as scattering in the small size parameter regime $\alpha \ll 1$. Scattering from larger spherical particles is explained by the Mie theory for an arbitrary size parameter α. For small α the Mie theory reduces to the Rayleigh approximation. The amount of Rayleigh scattering that occurs for a beam of light depends upon the size of the particles and the wavelength of the light. Specifically, the intensity of the scattered light varies as the sixth power of the particle size, and varies inversely with the fourth power of the wavelength. The intensity I of light scattered by a single small particle from a beam of unpolarized light of wavelength λ and intensity I_0 is given by:

$$I = I_0 \frac{1+cos^2\theta}{2R^2}\left(\frac{2\pi}{\lambda}\right)^4\left(\frac{n^2-1}{n^2+2}\right)^2\left(\frac{d}{2}\right)^6 \tag{2.14}$$

there R is the distance to the particle, θ is the scattering angle, n is the refractive index of the particle, and d is the diameter of the particle.

$$\sigma_s = \frac{2\pi^5}{3}\frac{d^6}{\lambda^4}\left(\frac{n^2-1}{n^2+2}\right)^2 \tag{2.15}$$

The Rayleigh scattering coefficient for a group of scattering particles is the number of particles per unit volume N times the cross-section. As with all wave effects, for incoherent scattering the scattered powers add arithmetically, while for coherent scattering, such as if the particles are very near each other, the fields add arithmetically and the sum must be squared to obtain the total scattered power.

Rayleigh scattering also occurs from individual molecules. Here the scattering is due to the molecular polarizability α, which describes how much the electrical charges on the molecule will move in an electric field. In this case, the Rayleigh scattering intensity for a single particle is given by

$$I = I_0 \frac{8\pi^4\alpha^2}{\lambda^4 R^2}(1 + cos^2\,\theta) \tag{2.16}$$

The amount of Rayleigh scattering from a single particle can also be expressed as a cross section σ. For example, the major constituent of the atmosphere, nitrogen, has a Rayleigh cross section of 5.1×10^{-31} m^2 at a wavelength of 532 nm (green light).[4] This means that at atmospheric pressure, about a fraction 10^{-5} of light will be scattered for every meter of travel. The strong wavelength dependence of the scattering ($\sim\lambda^{-4}$) means that shorter (blue) wavelengths are scattered more strongly than longer (red) wavelengths. This results in the indirect blue light coming from all regions of the sky. Rayleigh scattering is a good approximation of the manner in which light scattering occurs within various media for which scattering particles have a small size parameter. However, the pure amount of scattered light as part of the incident beam is strongly dependent on the wavelength, this phenomena is shown in figure 2.4.

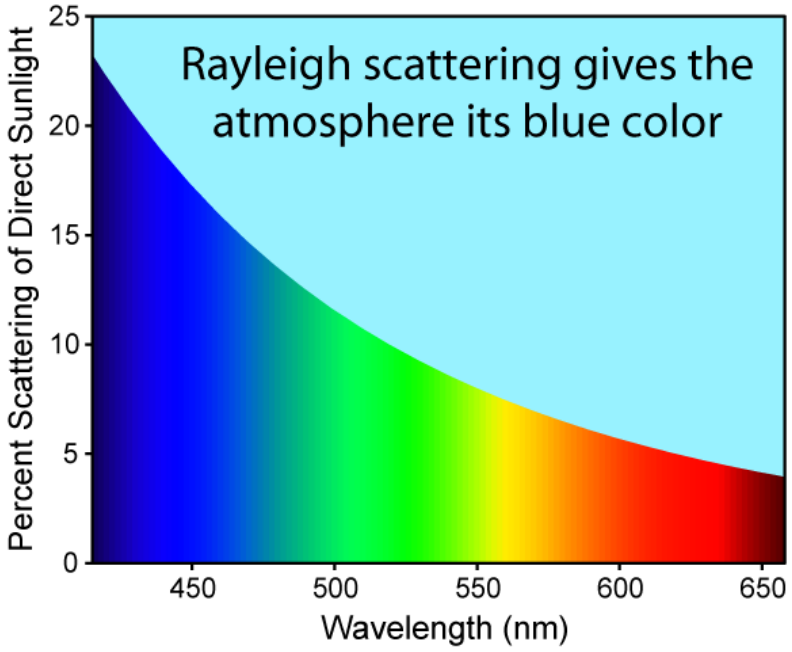

Figure 2.4.: Figure shows the percent of the incident light that is scattered, [28]

2.2.4 Mie Scattering

There is a gradual transition from Rayleigh to Mie scattering as the particle size increases, whereas the scattering pattern of Rayleigh is symmetrical and comparatively simple, the scattering pattern of Mie scatterers gets more complex with increasing particle sizes, as it is shown in figure 2.3 on page 10. Also with size increase, there is a noticeable increasing ratio of forward scattering to backscattering, which results in a growth of the forward lobe, also shown in figure 2.3. The dependency of scattering on wavelength, however, becomes much less significant. As may be inferred from the generally white appearance of clouds, since the water droplets in clouds exceed the size of Rayleigh scatterers by several orders. The present theory has been developed by many workers, all based on the initial researches of Mie(1908), much of it was anticipated by Lorentz in the period 1890 to 1900 which is why the theory is sometimes called Mie- Lorentz theory. Likewise as for the Rayleigh theory a spherical scatterer is assumed. Non spherical would be very complex and depend on the angle of the incident light to the particle orientation in space. Non spherical particles are therefore not in the scope of this thesis, when considering water droplets in liquid state, they are approximately spherical anyway. Mie scattering by a single oscillator is closely related to the scattering principle introduced for Rayleigh scattering and thus based on electromagnetic waves interacting with a dipole oscillator. Although the physical basis has been shown already in the Rayleigh scattering section, the Mie theory is more complex in detail, thus the reader may be guided directly to the scattering functions for mono dispersions of spherical oscillators.

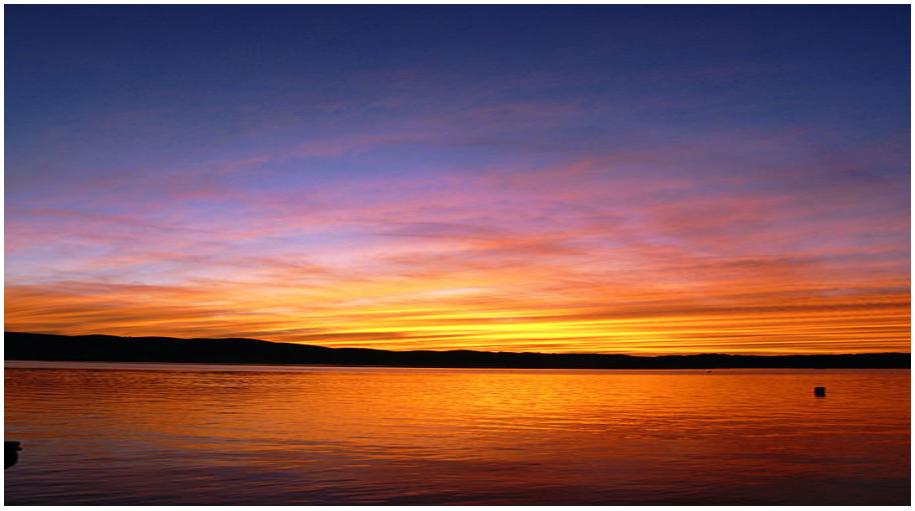

Figure 2.5.: The change of sky colour at sunset [31]

The change of sky colour at sunset (red nearest the sun, blue furthest away) is caused by Rayleigh scattering by atmospheric gas particles which are much smaller than the wavelengths of visible light. The grey/white colour of the clouds is caused by Mie scattering by water droplets which are of a comparable size to the wavelengths of visible light.

2.3 Koschmieder's Theory

In this section, the information of the atmosphere is put together to a holistic theory of horizontal visibility through the atmosphere. H. Koschmieder in 1924 was the first who was able to go beyond, from the Mie scattering theory to the "Theorie der horizontalen Sichtweite". This chapter describes his theory in detail, beginning with a concept called the *air light*.

2.3.1 The Air-Light

Air light is an important concept, that is known to everyone, however not always by this name, who observed a natural or urban extensive landscape from an elevated point. The observer will notice that those parts of the foreground that are closer to the horizon will be lighter in tone than those closer to the observer, this effect becomes more apparent the further away the objects are until they eventually blend into the horizon sky and become invisible. This way, even a black object becomes lighter and even appears in the same colour as the sky when it is seen far enough from the observer. The source for this increase in luminance with distance is of course the sunlight which is scattered into the eyes of the observer from the air, that is in the line of sight between him and the observed object. This phenomenon has been known for a long time and was used by painters for hundreds of years, the first quantitative analysis however was made by Koschmieder in 1924.

2.3.2 "Theorie der horizontalen Sichtweite"

Koschmieder published his "Theorie der horizontalen Sichtweite", which is German for theory of the horizontal visual range, in an extensive paper. The essentials of it are presented here. Koschmieder made some not too restrictive but simplifying assumptions that can be summarised as in the following enumeration:

1. "The atmosphere is considered to be a turbid medium, containing a large number of small particles."

2. "Each element of volume contains a very large number of particles, and each particle of a much smaller order of magnitude than the element itself."

3. "The scattering action by each particle is independent of the presence of all the other particles."

4. "The light scattered from an element of volume is considered to coming from a point source of which the intensity is proportional to the number of particles."(This is equivalent to the assumption that the light from various particles is incoherent, which means that there is no stable phase relation.

5. "Light rays are to be considered as rectilinear, that is to say that atmospheric refraction will be neglected."

6. "Every part of the sky is equally illuminated.

Later, the earlier assumptions made by the physicist Gruner (1919) were found convenient for this theory and have thus been added:

7. "The coefficient of attenuation by scattering, β, is constant in a horizontal plane, in particular near the surface of the earth, where it takes the value β_0."(Despite the earlier argumentation, in practice this is approximately true in the atmosphere for a defined location, as particle size distribution is mostly a function of altitude and can therefore be assumed constant for a constant altitude.)

8. "The curvature of the earth is neglected, and its surface is considered as plane, horizontal, and diffusely reflecting"(Which is approximately the case for visual ranges anyway.)

9. "The linear dimensions of the whole observed object are small in comparison to its distance from the observer." With image dehazing in mind, the seventh assumption implies that this theory cannot be used for images taken from satellites or other aerial photography such as from a plain downwards. However it is possible to dehaze those types of images too, admittedly with slight alterations to the theory.

After Koschmieder made the initial assumptions, he integrated the illumination over a cone of air, illuminated by the diffuse sky light, the diffuse ground light and the sun directly, as shown in figure 2.6.

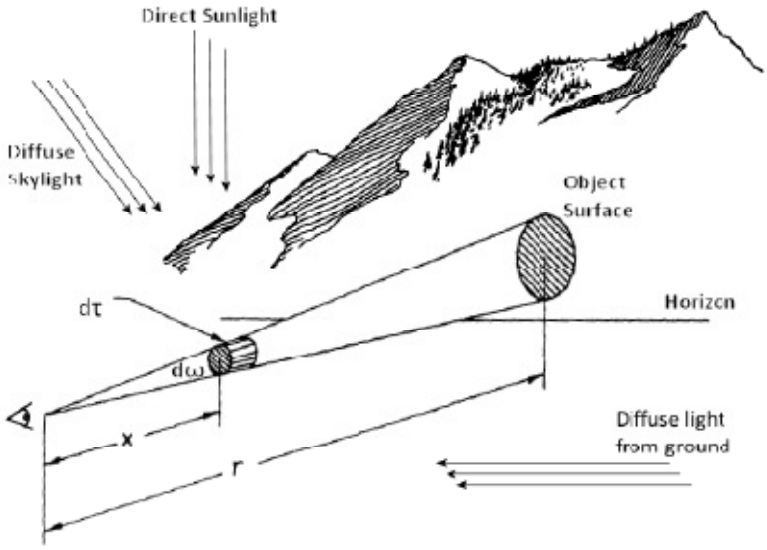

Figure 2.6.: Illustration for Koschmieder's theory, showing the volume element $d\tau$. [6]

Although it would exceed the boundaries of this thesis to follow him through the entire integrations, the most important steps are summarised. He considered an element:

$$d\tau = d\omega \cdot x^2 dx \tag{2.17}$$

for the cone of air, as in figure 2.6 and the object being a black object rising above the horizon at distance *r*. The observer being at $x = 0$. Now for any given value of ϕ the scattering function $\beta(\phi)$ will be proportional to the scattering coefficient β (see equation 2.12, page 11), therefore for the particular distribution of incident illumination, the intensity of the volume element $d\tau$ in the direction of the eye will be

$$dI = d\tau \cdot A\beta \tag{2.18}$$

With *A* a constant of proportionality, to be determined from boundary conditions, as it will be shown next. According to Koschmieder, the illuminance *L* of the scene at the eye due to the scattered light by the air from $d\tau$ is

$$dL = dI.x^{-2}.e^{-\beta x} \tag{2.19}$$

Here $e^{-\beta x}$accounts for the transmittance of the thickness x of the atmosphere. When considering the solid angle $d\omega$ within the volume element $d\tau$, the equation becomes

$$dL = \frac{1}{d\omega} dI . x^{-2} . e^{-\beta x} \tag{2.20}$$

or writing dI in terms of x and $d\omega$, it is

$$dL = A\beta e^{-\beta x} dx \tag{2.21}$$

which can be integrated over the entire cone to get the apparent luminance of the object

$$L_\beta = \int_0^r A\beta e^{-\beta x} dx = A\left(1 - e^{-\beta r}\right) \tag{2.22}$$

This is the A as it was referred to earlier. Supposing a black object is infinitely far away, then the value of its luminance will converge to the luminance value of the horizon sky L_h. Thus

$$L_h = \int_0^\infty A\beta e^{-\beta x} dx = A \tag{2.23}$$

And therefore

$$L_\beta = L_h\left(1 - e^{-\beta r}\right) \tag{2.24}$$

This is probably the most important formulation in Koschmieder's theory, however this is only true for a black object, that is to say, none of the luminance actually originated at the object itself. This condition is rather impractical, fortunately with a slight alteration, the formula can account for an object having a luminance L_0.

$$L = L_0 e^{-\beta r} + L_h\left(1 - e^{-\beta r}\right) \tag{2.25}$$

With equation 2.56 the theory is very close to a form which can be used directly in applications, however not quite there, since it does not take into account the absorption by the atmosphere. Because absorption is often of comparable magnitude to scattering, the extinction coefficient (equation 2.16, page 30) is used in the following formula:

$$L = L_0 e^{-(\beta+k)r} + L_h\left(1 - e^{-(\beta+k)r}\right) = L_0 e^{-\sigma r} + L_h(1 - e^{-\sigma r}) \tag{2.26}$$

As a side note, when using $\beta + k$ it is also called the "two-constant theory".

2.3.3 Importance of Koschmieder's Theory

As we know, the decrease in contrast directly causes a lower visibility. This is now, thanks to Koschmieder, quantifiable. Let L_0 and L_0' the luminances of two objects at close distance, then it is at distance R:

$$L_R + L_R' = (L_0 - L_0')e^{-\sigma R} \tag{2.27}$$

now using the contrast, as defined by

$$C_0 = \frac{L_0 - L_0'}{L_0'} \tag{2.28}$$

which is the *inherent contrast*, and

$$C_R = \frac{L_R - L_R'}{L_R'} \tag{2.29}$$

that is to say the *apparent contrast*. Now equation 2.27 may be written as

$$C_R = C_0 \left(\frac{L_0'}{L_R'}\right) e^{-\sigma_0 r} \tag{2.30}$$

This formula is the law of contrast reduction as it was discovered by Duntley (1948) [6]. Koschmieder's theory has been verified by many field studies to contrast and visual range since its development.

CHAPTER 3

DEHAZING METHODS

Many dehazing algorithms have been developed by different workers that were very active in this field of study in recent years. This chapter will describe the theoretical principles and main differences between these methods.

3.1 Overview of Dehazing Methods

To achieve the goal of haze removal and visibility improvement, several ways can lead to decent results. The methods can basically be divided into two groups, those methods that only need one single image for dehazing and those methods using two or more input images for one dehazed image. Also, there are model based methods and those trying to enhance the contrast of an image using simpler computer vision techniques such as gamma correction, unsharp masking or histogram equalisation.

The model based methods usually produce a depth map of the scene as a byproduct, the variety of applications that could make use of the depth information seems to be endless, Kopf et al.(2008) [8] explored some possibilities in their paper. The question of what method gives the best visibility improvement should best be answered by the human, as he will be the ultimate judge using the dehazed image in applications such as surveillance scenarios. It should therefore be evaluated in psychological studies, testing the probability of detection and employing measurements of tiredness of the eyes using the one or the other dehazing method. A comparison of a broad variety of methods can be seen in figure 3.1, the images are taken from [4].

Figure 3.1(a) shows the input image, right next to it in 3.1(b) is the result of a polarisation based dehazer, due to its outstanding image quality this method can be seen as reference method. The next row 3.1(c)-(e) contains images, whose visibility have been improved by simpler image processing methods such as gamma correction, histogram equalisation and unsharp masking, respectively. The last row contains the results of Fattal(2008) [4] and Chavez(1988).

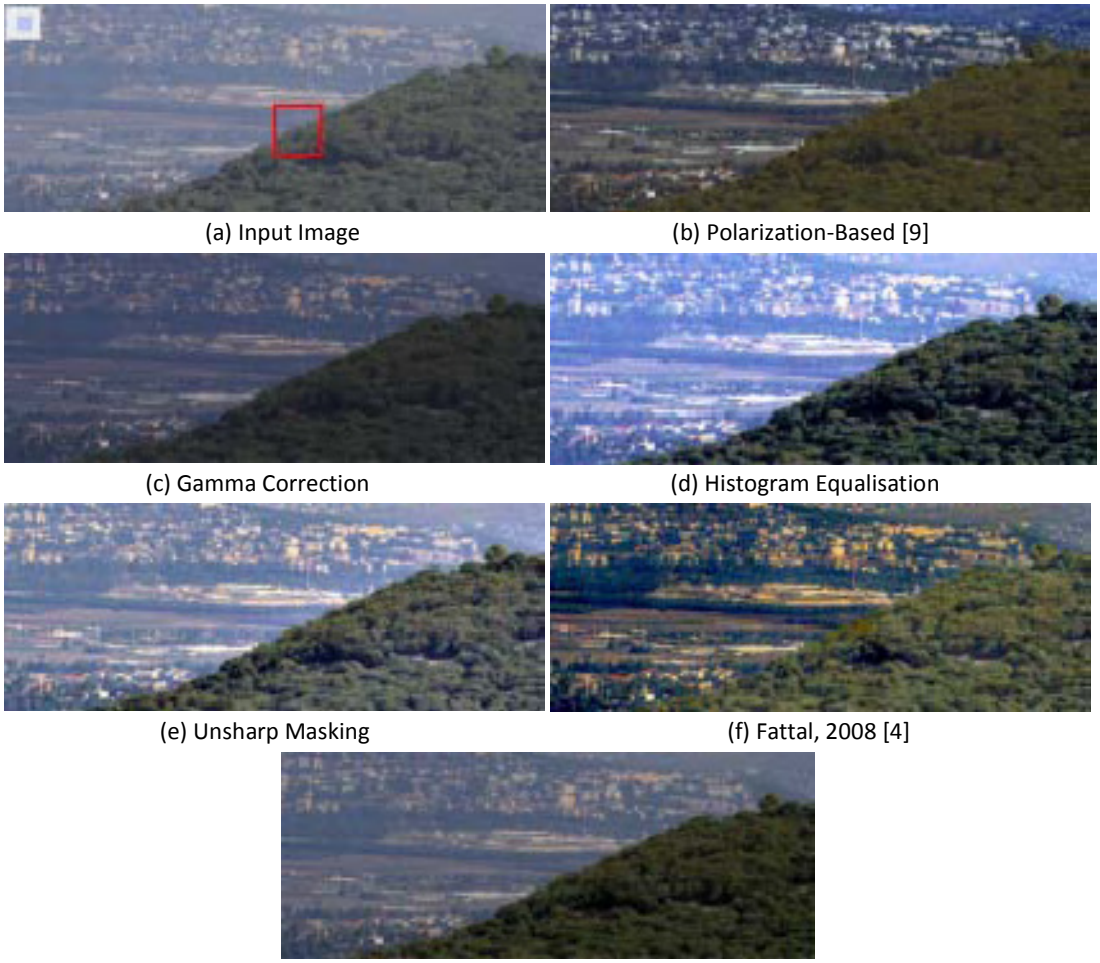

(a) Input Image (b) Polarization-Based [9]

(c) Gamma Correction (d) Histogram Equalisation

(e) Unsharp Masking (f) Fattal, 2008 [4]

(g) Dark Channel Subtraction

Figure 3.1.: Comparison of computed images from the same input image created with different dehazing techniques. [4]

Fattal's results are the best for the single image dehazing methods in this comparison, which shows that single image model based, recently developed methods are the way to go. As of three years prior the time of writing this thesis, a couple of works with outstanding results have been published. He et al. [2] have published a new method based on the dark channel subtraction from Chavez(1988), that produces comparable results to those of Fattal. Also Tan [10] and Kopf et al. [8], respectively, have worked in dehazing field with their own proposed methods. The latter gives outstanding results, and is one of the best in quality available today. These four works are compared in the figure 3.2 and 3.3 , the images are from [11].

(a) Input Image (b) Tan, 2008 [10]

(c) Kopf et al., 2008 [8] (d) Fattal, 2008 [4]

Figure 3.2.: Comparison of computed images from the same input image created with different model based single image dehazing techniques. [11]

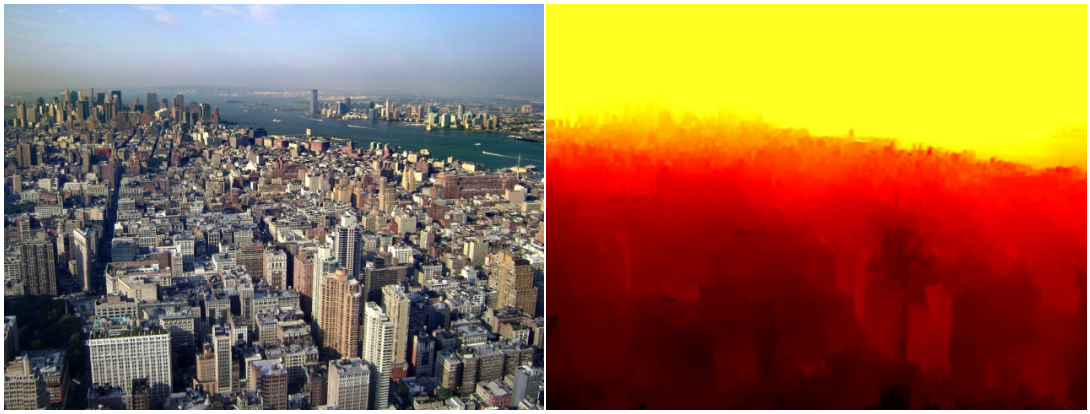

(a) He et al., 2010 [2] (b) He et al., 2010 [2]

Figure 3.3.: The figure(a) shows dehazing result using the algorithm of [He et al., 2010a], using 3.2a as input image. Figure (b) shows the depth map of the scene computed using the same algorithm. [11]

It is worth mentioning, that all dehazing methods no matter what principle they use, depend somewhat on the dynamic range of the image sensor itself. This is a limiting factor, less in CCDs and more in CMOS sensors but present in all today's available image sensors. Image quality, especially the contrast could be enhanced when using higher dynamic range sensors [1].

It will now be drawn attention to each one of the introduced methods in order to find out the method with the most potential for real-time applications without sacrificing too much of the image quality of the respective dehazing method.

3.2 Non-Model-Based Contrast Enhancer

The middle row in figure 3.1 shows the results of the non model based contrast enhancers. The striking similarity is the blue hue that the three have in common, this is the typical blueness of small haze particles as described in the preceding chapter. This can only be eliminated with model based techniques. These are just a few examples, there are actually many contrast manipulation algorithms available, mostly known from photography. As we know that humans have a minimum contrast threshold that is needed for object separation. Luckily, this contrast threshold can be raised in images using simple mathematical concepts like the gamma correction, unsharp masking or histogram equalisation. These were not developed for image dehazing, can however improve visibility. Thus these methods can also be used to further improve an already dehazed image. Thus for this purpose, they shouldn't be used exclusively, but in combination with a dehazer. For the sake of completeness however, the three introduced concepts will now be described very briefly.

3.2.1 Unsharp Masking

The idea behind unsharp masking is to emphasise edges. An unsharp masking algorithm can detect edges and alter the levels of brightness on both sides of the edge in a way that the darker side gets even darker towards the edge and the lighter parts get even lighter towards the edge [12]. This produces an overshoot and an undershoot, respectively of the brightness curve of the pixels at the edge. This is illustrated by figure 3.4. An unsharp mask amplifies high-frequency components. This results in a better sharpness of the

image, thus raising the contrast locally. The ideal brightness curve would be a step function, as illustrated by the right plot in figure 3.4.

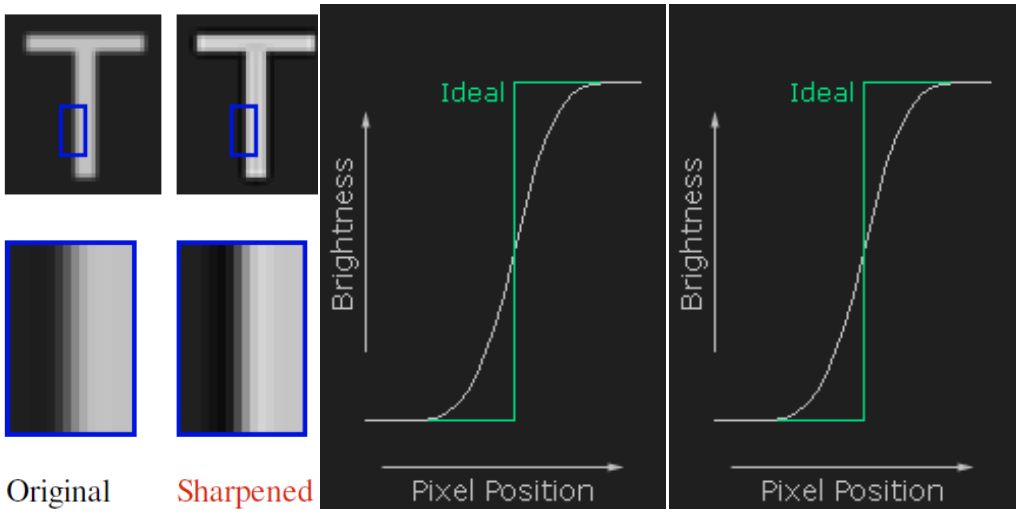

Figure 3.4.: Shows the principle of unsharp masking, left plot shows the overshoot and undershoot resulting from the masking versus the actual brightness curve, right plot shows the ideal rectangular curve versus the actual curve of the input image. [12]

3.2.2 Gamma Correction

Gamma correction refers to a nonlinear operation that amplifies or reduces the luminance intensity of an image. This operation is performed on each pixel in the same way, no matter its original value. By lowering in the power-law expression for the gamma correction:

$$B_{out} = B_{in}^{\gamma} \tag{3.1}$$

the contrast levels may be raised in dark images with low contrasts. Here B_{in} and B_{out}, respectively denote the Brightness levels before and after the gamma correction. The principle of gamma correction can be seen in the plot of figure 3.5, the input brightness curve is here as an example the input of a CRT display with $\gamma = 2.2$, with a gamma correction curve of $\gamma = 1/2.2$ the actual linear curve of interest can be restored. The ordinate shows the input value(brightness) and the abscissa shows the output value(brightness).

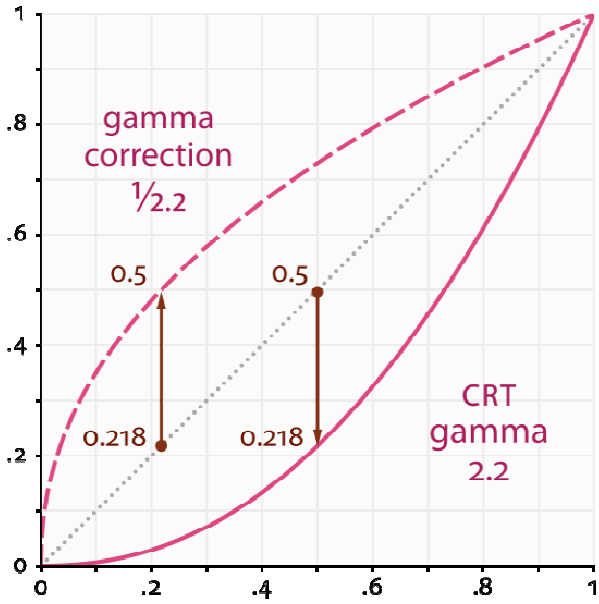

Figure 3.5.: Plot shows the principle of gamma correction, [29]

3.2.3 Histogram Equalisation

The histogram equalisation is a method using the image's histogram in order to improve contrast. Since only so much of brightness values can be displayed, all gradations of brightnesses and therefore contrasts must be within the brightness bandwidth. Thus the best results can be obtained, when spreading out the most frequent intensity values over the entire histogram.

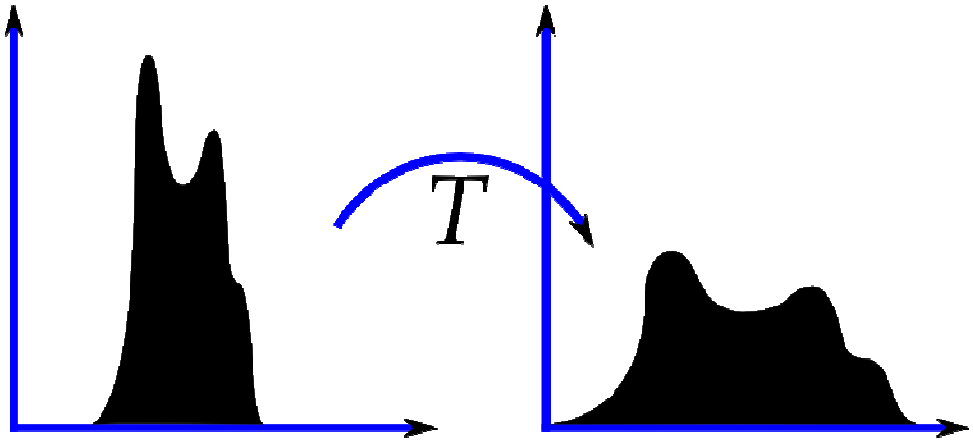

Figure 3.6.: Plot shows the principle of histogram equalisation, the abscissa denotes the brightness values. The ordinate denotes the frequency that x-value is used. [30]

A disadvantage of this method is that it may increase the noise by discriminating it from the actual usable signal. However, this method is one of the more advanced methods to improve image contrast, and is of the three mentioned in this thesis the most resource intensive, but usually also the one with the best results. Figure 3.6 illustrates the basic idea behind histogram equalisation. The left plot shows the input, where not all possible brightness values are used and the right plot after the transmission. This method generally improves the global contrast, locally however spots in the image with close brightness values may not be improved in some cases.

3.3 Polarisation Based Visibility Improvements

Polarisation-based dehazing methods are part of the multi-image group, they usually use two input images taken with two differently polarised filters, one after another, to produce one dehazed image. This technique makes use of the fact that the airlight is at least partially polarised(see section 2.2, page 27), whereas the direct transmission of the object is unpolarised. Polarisation filters alone cannot eliminate haze in scenes, at least two images with different polarisation filter states are necessary. The assumed model is that of Koschmieder's theory with additional polarisation filters, see figure 3.7.

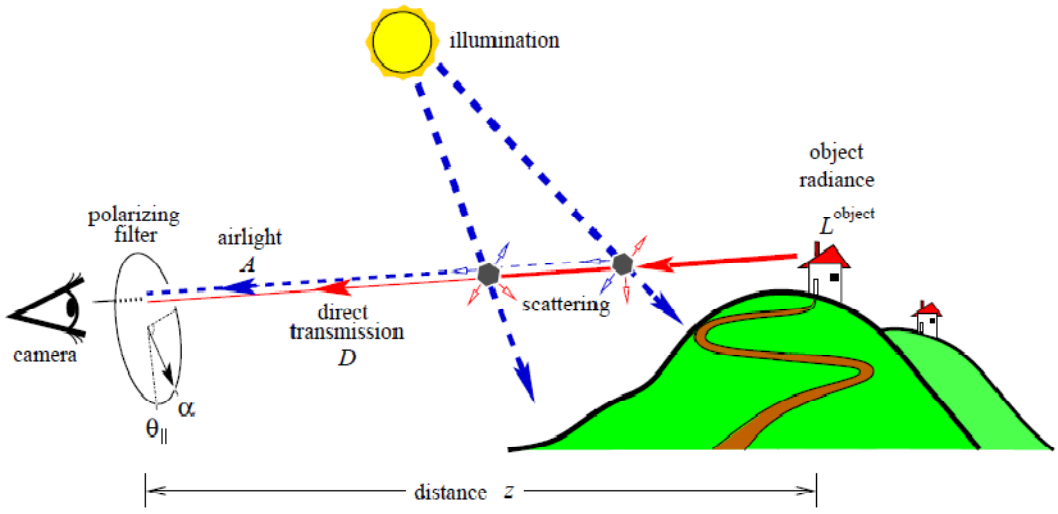

Figure 3.7.: Model for polarisation-based dehazing. [1]

With the knowledge from the preceding chapter, this figure is pretty much self-explanatory. In this section, the basic principles ae described behind the method shown in [1], however this is also representative for all other known polarisation-based methods.

Consider figure 3.7, the resulting image of a scene consists of two main components, the first coming from the object radiance L^{object} and the second from the airlight A. The former is free of scattering in the line of sight and is only dependent on the attenuation of the atmosphere. The direct transmission $t(x)$ can then be written as:

$$t(x) = L^{object}.\tau \tag{3.2}$$

where

$$\tau = e^{-\beta d(x)} \tag{3.3}$$

is the transmittance of the atmosphere. Here $d(x)$ denotes the distance from the camera

to the object and β the attenuation coefficient. The airlight, also called the *path radiance*, is produced by the scene illumination and given by:

$$A = A_{\infty}(1 - \tau) \tag{3.4}$$

where A_{∞} is the saturation airlight, which depends on the atmospheric and illumination conditions. It is the maximal possible intensity of airlight, which corresponds to the airlight of the sky near the horizon. In contrast to the direct transmission the airlight factor increases with distance and dominates the image irradiance I_{total} at long ranges:

$$I_{total} = t(x) + A \tag{3.5}$$

This is the major cause for reduction of image contrast in haze. The partially polarised airlight can now be used to restore a haze free image by mounting a polarisation filter with angle α in the imaging system. When rotating the polariser, there is an orientation at which the image is least intense, let this be denoted by I_{min}. I_{min} corresponds to the lowest amount of airlight. This orientation of the polarisation filter may be denoted by $\theta_{\|}$. When now rotating the pol. filter by 90° relative to $\theta_{\|}$, then the image irradiance is strongest, since now the principle polarisation component of the airlight is strongest, this may be called I_{max} with $\theta_{\perp}$. Once these two images are acquired, the dehazed image can be estimated by:

$$\hat{L}^{object} = \frac{I_{total} - \hat{A}}{\hat{\tau}} \tag{3.6}$$

where the estimated transmittance, $\hat{\tau}$ is:

$$\hat{\tau} = 1 - \frac{\hat{A}}{A_\infty} \tag{3.7}$$

and the estimated airlight $\hat{A}$ is:

$$\hat{A} = \frac{I_{max} - I_{min}}{p} \tag{3.8}$$

Here p is the degree of polarisation of airlight, which depends on the particle size of the aerosols. It can however be estimated with just the parameters already known. It is measured from the raw images by looking at pixels which correspond to objects at infinity, naturally such pixels are those of the sky near the horizon(in later years, Schechner et al. proposed ways to find p without having a horizon in the picture).

$$p = \frac{I_{max} - I_{min}}{I_{max} + I_{min}} \Big|_{d(x)=\infty} \tag{3.9}$$

Hence the airlight saturation value can be estimated from the same sky area as

$$A_\infty = [I_{max} + I_{min}]_{d(x)=\infty} \tag{3.10}$$

As stated in section 3.1, the distance map can be recovered as a byproduct:

$$\beta \hat{d}(x) = -\log\left[1 - \frac{\hat{A}}{A_\infty}\right] \tag{3.11}$$

This operation must be done for each color channel separately. The method works with only slight alterations for both atmospheric photography [13] as well as for underwater photography [14]. Problematic however, are surfaces that are specular, like windows or water, because they reflect partially polarised light and lead to errors in the calculation. These areas must be treated separately, and can for example be detected by analysing inconsistencies in the depth map,[1].

Although this method is model based, no knowledge about the actual scattering particles is necessary. However, due to its basic principle, only Rayleigh scattering can properly be eliminated. Since Mie scatterers polarise the light in a different way if any (the larger the particle, the less the polarisation). Also clear day recording is preferred for this method, since then the airlight polarisation can properly be separated from the direct transmission.

However, when the prerequisites have been met, polarisation-based dehazing gives very good results, an example is given in figure 3.8. Note that the correct colours can also be restored in contrast to the formerly mentioned enhancers that purely focus on the contrast without being model based.

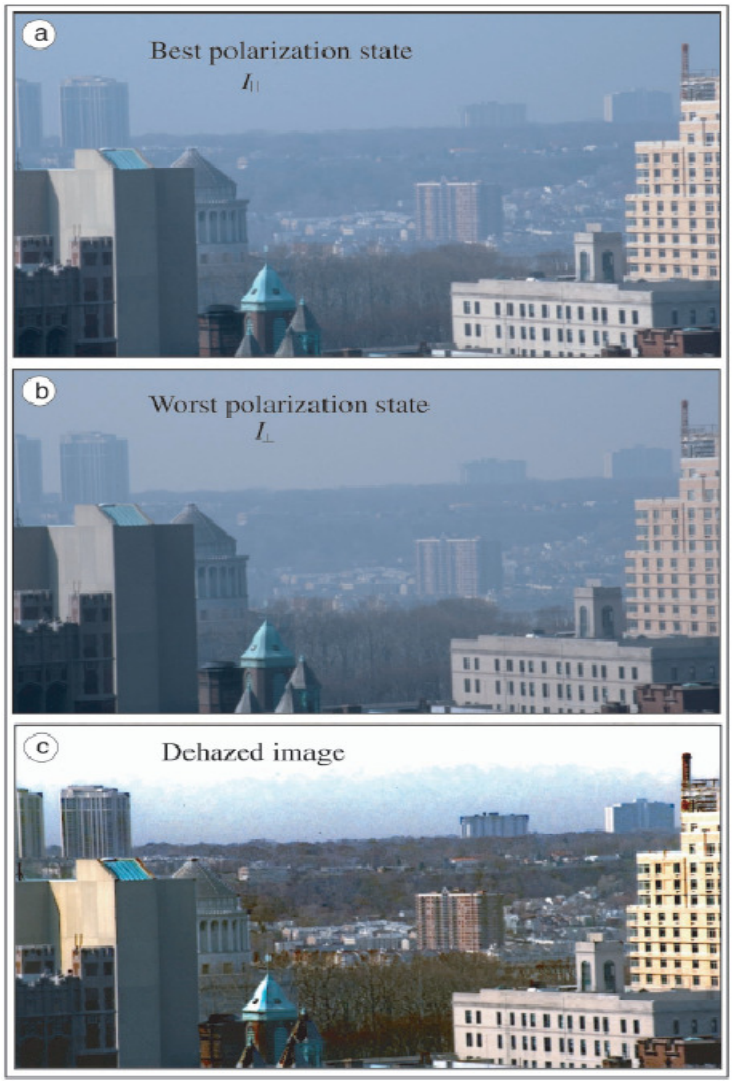

Figure 3.8.: Example for polarisation-based dehazing, (a) shows the image taken with a polarisation filter under best polarisation state $\theta_{\|}$, (b) shows the image taken with a polarisation filter under worst polarisation state $\theta_{\perp}$ and (c) shows the dehazed image. [13]

Multi-image dehazing methods in general, although usually giving qualitatively great results tend to be unsuitable for real-time image dehazing purposes. It is thinkable that for example, half the frame rate could be sacrificed in order to capture two images with different polarisation state, however rotating a static polarisation filter is of course very

slow when done by hand or even done by a clocked mechanical mechanism. Although there are now electronic liquid crystal based polarisation filters available on the market that may be able to switch on every frame, they are very colour selective and give different results for different wavelengths of light [1]. Namer and Schechner also stated, that: "While we still do not demonstrate dehazing in video, we currently assess the LC technology using still photography." [1]. Also there is the argument, that special hardware requirements may not be feasible in real world applications, since it may be inconvenient in practice to equip once deployed cameras with a liquid crystal polarisation filter for simple physical or monetary reasons. Especially in windy weather conditions, cameras that are mounted on high masts and equipped with a polarisation filter may be very sensitive to translation. Thus two images of different polarisation state may be useless when shifted by a few pixels or even subpixels due to wind or other causes(e.g. engine turbines of large air crafts causing low frequent vibrations in airport surveillance environments). Additionally to multi-image techniques, there are methods using multiple images such as the dehazing method of Nayar and Narasimhan described in [15] and [16], which require images taken under two different weather conditions. This is of course way too slow for real-time applications.

3.4 Fattal's Method

Fattal introduced a new technique in 2008 for single image dehazing that produces qualitatively great results on hazy images. The main idea of this approach is to take the image degradation model from Rossum and Nieuwenhuizen([17]) also known as the *Radiative Transport Equation*(shown in 3.12) and express it in terms of surface shading in addition to the transmission. This gives a refined image formation model. Quoting Fattal: "This allows us to resolve ambiguities in the data by searching for a solution in which the resulting shading and transmission functions are locally statistically uncorrelated. A similar principle is used to estimate the color of the haze." [4].

$$I(x) = t(x)J(x) + \big(1 - t(x)\big)A \tag{3.12}$$

In this equation, $t(x)$ is the transmission, a scalar for each colour component:

$$t(x) = e^{-\beta d(x)} \tag{3.13}$$

Similar to the preceeding section the term $t(x)J(x)$ is being called the direct attenuation and $(1-t(x))A$ the airlight. Here $I(x)$ is the input image, $J(x)$ the haze free image and A the global atmospheric light colour vector. This equation is commonly used to describe the image formation in the presence of haze and was used before by, for [15] and [18]. This inherits many ambiguities in each pixel independently, such as in the airlight-albedo, that gives a large degree of freedom. Fattal however, manages to reduce this degree: "To reduce the amount of this indeterminateness, we simplify the image locally by relating nearby pixels together." [4]. He does that by grouping pixels belonging to the same surface, thus having the same surface reflectance and therefore the same constant surface albedo. Now the key idea to resolve the airlight-albedo ambiguity is that he assumes that the surface shading l and the scene transmission t are statistically uncorrelated, because l depends on the illumination on the scene, surface reflectance properties and the scene geometry, whereas t depends on the density of the haze (β) and the scene depth. Fattal then presents an independent component analysis method to determine l and t.

The same principle of uncorrelation is applied to the estimation of the airlight colour. This method also gives a depth map, which could be used over and over again for a static camera when using it in a real-time application. "The Method works quite well for haze, but has difficulty with scenes involving fog, as the magnitude of the surface reflectance is much smaller than that of the airlight when the fog is suitably thick." [19]. According to Fattal, the noise level in the input image influences the quality of the dehazed image greatly. However, with Fattal's method the absolute error in transmission and haze-free image are both less than 7% in tests where the real haze free image was known, explanatory: "In its essence this method solves a non-linear inverse problem and therefore its performance greatly depends on the quality of the input data." [4]. "Moreover, as the statistics is based on color information, it is invalid for grayscale images and difficult to handle dense haze which is often colorless and prone to noise." [2]. For examples of performance, please refer to figure 3.1 and figure 3.2.

3.5 Tan's Method

Tan presented a single image based dehazing method in 2008, too. His proposed method is based on the optical model:

$$I(x) = L_{\infty}\rho(x)e^{-\beta d(x)} + L_{\infty}\left(1 - e^{-\beta d(x)}\right) \tag{3.14}$$

with L_∞ being the atmospheric light and $\rho(x)$ the reflectance, this formula is very similar to Koschmieder's equation 2.25(on page 18). The first term in this equation is the direction attenuation and the second term corresponds to the airlight *A*. He then expresses it in terms of light chromaticity and as a vector for the colour components. In this formula are more unknowns than knowns. Nevertheless, there are some clues or observations that Tan makes use of in his algorithm:

1. "The output image, must have better contrast compared to the input image **I**." [10]
2. "The variation of the values of A[atmospheric light for the colour components] is dependent solely on the depth of the objects, *d*, implying that objects with the same depth will have the same value of A, regardless their reflectance (ρ). Thus, the values of A for neighbouring pixels tend to be the same. Moreover, in many situations A changes smoothly across small local areas. Exception is for pixels at depth discontinuities, whose number is relatively small." [10]
3. "The input images that are plagued by bad weather are normally taken from outdoor natural scenes. Therefore, the correct values of (the direct attenuation) must follow the characteristics of clear-day natural images." [10]

The author of this paper([10]) then proposes an algorithm employing the clues above. With **I** being the input image, the algorithm is:

1. Estimate L_∞
2. Compute α (light chromaticity) from L_∞
3. Remove the illumination colour of **I**
4. Compute the data term $\phi(A_x|A_y)$ from **I'**
5. Compute the smoothness term ψ (A_x,A_y)
6. Do the interference, which yields the airlight, A
7. Return the direct attenuation, $D\gamma'$, computed from A.

He also proposed a data cost function for step 4 in the framework of Markov random fields, which can be efficiently optimised by various techniques, such as graph-cuts. This algorithm is applicable for both colour and gray images. However, it does not recover the scene's original colour [10]. Despite its neat approach, this method is not easily applicable to real-time applications since it takes "The computational time for 600x400 images, using double processors of Pentium 4 and 1 GB memory, approximately five to seven minutes

(applying graph-cuts with multiple labels)" [10]. Also, this method has some flaws compared to other methods of for example Fattal and Kopf et al. in terms of image quality. Since it produces halos near depth discontinuities and "The method tends to produce over enhanced images in practice." [19]. As an example for Tan's method in terms of image quality, please refer to figure 3.2.

3.6 The Deep Photo System

A rather different approach was proposed by Kopf et al. in 2008 called the *Deep Photo System*. Crucial to all dehazing methods is to acquire the depth information of every pixel in the frame, but rather than acquiring these by making assumptions or employing statistical observations, Kopf et al. developed a data-driven dehazing procedure, by employing a registration process to align the photograph within an existing 3D model. This way the method does not need to estimate the distances in the scene, but will get the exact distances right away, assuming that such kind of georeferenced digital terrain and urban models are available. They propose a user interactive referencing system, in which the user registers certain scene points with the corresponding points in the model, such a model could come from satellite image data obtained from GoogleEarth™, BingMapsTMor other providers. The 3D models for buildings and other objects are already available for many cities like Berlin or New York City and others(for example through VirtualEarth™). Additionally helpful can be GPS tags, produced by the imaging system itself, sometimes even tilt and heading is provided by these cameras. With a static surveillance camera in mind, the scene must be geo-referenced only once initially and could then rely on a set of depth information indefinitely assuming no camera shifts take place. Taking airports as an example, 3D models of buildings and high resolution geo information is usually available due to construction plans and air traffic controlling agencies. Here also lies the limitation of such a system, since it heavily relies on those sets of data, if no 3D model of the scene is available, no dehazing can be performed. Also in dynamic scenes, with vehicles such as aircrafts driving or flying through, there is no depth information for those foreground objects whatsoever, hence dehazing for those objects would rely on wrong depth information and cause a superabundant dehazing on those spots. However, for scenes where distances are great and the influence of moving objects to scene distance is low, such as in figure 3.2, the image quality is remarkable.

After acquiring the depth information, the method of Kopf et al. estimates the airlight and the attenuation coefficient similarly to the other haze removal methods and then basically solves Koschmieder's equation, however with some nuances differently. In the paper [8], the authors explore further possible applications for the depth information of an image, other than dehazing, such as approximating changes in lighting, expanding field of view, adding haze, adding new objects into the image with the correct haze values according to distance, and integration of GIS data into the photo browser, just to name a few. Since often the depth map of other dehazing methods also comes as a byproduct, these mentioned applications may also be implemented combined with other dehazers, such as [4] or [2], for example. Problems may arise from the fact that the alignment between the photograph and the model may not be completely accurate due to unprecise 3D models or the lens curvature of the imaging system.

3.7 Improved Dark Object Subtraction

The *Dark Object Subtraction* is a method widely used in multi-spectral remote sensing systems and an improved version of it was inspiring for the dehazing method in the next section, the *Dark Channel Prior*, which is why DOS(Dark Object Subtraction) will now be summarised briefly. The DOS was developed many years before the improved version, but is now almost entirely used in its improved version today, as it was introduced by Chavez in 1988. The main idea behind this method is that in a scene at least one dark object exists, that has zero reflectance(is black). Also any measured radiance is attributed to atmospheric path radiance only. This also means, that the atmospheric transmittance is not corrected. The method needs at first to identify a dark object in the scene and then estimate the atmospheric light, which is the additive term to the otherwise black pixel(if input image were haze free). This constant is then subtracted from all pixels in the image in order to remove the first-order scattering component.

However in satellite imaging, where this technique is mostly used, the imaging sensor usually provides multi spectral data, such as from the Landsat Thematic Mapper, thus in the improved version the spectral bands are no longer treated separately from the scattering properties but dependent on the specific wavelength-scattering relationship(see Mie Scattering, page 14), since atmospheric scattering is highly wavelength dependent. This leads to much better results when using colour images, since each colour band will have its own dehazing iteration. Chavez's method "allows the user to select a relative atmospheric

scattering model to predict the haze values for all the spectral bands from a selected starting band haze value. The improved method normalizes the predicted haze values for the different gain and offset parameters which are being used by the imaging system." This was also one of the first dehazing methods that does not need further information about the scene than those already contained within the image data. Difficulties arise in scenes where no dark object is present, which is a rare case in satellite images with large amounts of pixels, where it is statistically very likely to have also dark pixels, arising from shadowed areas. However these scenarios where dark objects are missing do exist. The performance of this method can be seen in figure 3.1.

3.8 Dark Channel Prior

The success of recently developed techniques such as [4], [8] and [10] compared to earlier dehazing methods lies in using stronger assumptions. A very promising new single image technology, developed in 2010 called the *Dark Channel Prior* comes from He, Sun and Tang. This method does not rely on significant variance on transmission or surface shading in the input image and the output image is less effected by halos than in [10]. Although every assumption limits the algorithm to specific use cases, the main assumption here seems to work for most outdoor scenes, except for those where "the scene object is inherently similar to the airlight over a large location and no shadow is cast on the object" [2]. The main prior in this method is, as the name lets assume, the dark channel prior, which is a statistical based assumption of haze-free outdoor images. The prior says, that in most of the local regions that aren't sky, very often some pixels have a very low intensity in at least one of its colour channels(RGB). In the hazy image then, these dark pixels can be used to determine the true airlight, since the airlight is apparent on a dark object(as stated in the preceding chapter). The dark channel J^{dark} of J(the haze-free image) is defined as

$$J^{dark}(x) = \min_{c\epsilon\{r,g,b\}} \left(\min_{y\epsilon\Omega(x)} \left(J(y) \right) \right) \tag{3.15}$$

where J^c is a colour channel of J and $\Omega(x)$ is a local patch centered at x. This statistical observation is called the *dark channel prior*. These low intensities come from natural phenomena such as shadows or just really dark or colourful surfaces. Since J^{dark} tends to

be zero and as A^c, the corresponding channel of the atmospheric light is always positive, it may be written:

$$J^{dark}(x) = \min_{c\epsilon\{r,g,b\}} \left(\min_{y\epsilon\Omega(x)} \left(\frac{J^c(y)}{A^c} \right) \right) = 0 \tag{3.16}$$

This can be used to estimate the transmission for that patch $\Omega(x)$ by putting 3.16 into the image formation model 3.12, however now in combination with the min operator:

$$\min_c \left(\min_{y\epsilon\Omega(x)} I^c(y) \right) = \tilde{t}(x) \min_{c\epsilon\{r,g,b\}} \left(\min_{y\epsilon\Omega(x)} (J(y)) \right) + (1 - \tilde{t}(x)).A^c \tag{3.17}$$

with $\tilde{t}(x)$ denoting the transmission in a local patch, then putting 3.16 into 3.17 leads to:

$$\tilde{t}(x) = 1 - \min_{c\epsilon\{r,g,b\}} \left(\min_{y\epsilon\Omega(x)} \left(\frac{I^c(y)}{A^c} \right) \right) \tag{3.18}$$

which is a direct estimation of the transmission for each local patch. They then apply a soft matting algorithm on the depth map, this leads to a much smoother and detailed depth map, an example of that can be seen in figure 3.3(b). Having the transmission or depth map, the scene radiance according to 3.12 can now be recovered. However, since the direct attenuation term $J(x)t(x)$ can be very close to zero, the transmission is restricted to a lower bound t_0 for example $t_0 = 0.1$, since the scene radiance is typically not as bright as the atmospheric light A. The final scene radiance $J(x)$ may then be recovered by:

$$J(x) = \frac{I(x) - A}{max(t(x), t_0)} + A \tag{3.19}$$

In the above calculations, the atmospheric light A was considered to be known, which is of course not the case, at least initially. Unlike other workers in the field, He et al. do not take the pixel with the highest intensity as the atmospheric light, since this could as well be a white surface such as a white airplane or a bright building very near. He et al. pick the top 0.1% brightest pixels in the dark channel ($\min_c(I_c)$), since these must be the most haze-opaque. Among these pixels, the pixel with the highest intensity in the input I is picked as the atmospheric light A. This may not be the brightest pixel in the image, but is more robust than the "brightest pixel" method according to [2]. This method seems very elegant and shows very good results, as one can see from figure 3.3.

3.9 Geometry Based Dehazing Methods

This technique described by [19] is more an improvement that can be used throughout all single image based dehazing methods than a dedicated image dehazing method itself. Thus this principle can be used in combination with the methods mentioned above. The authors Carr and Hartley investigated existing dehazing methods and introduced the idea of simplifying the depths map estimation by assuming a common geometry that applies for most outdoor surveillance scenarios. Their motivation can be best described by a citation: "Although each method (meaning existing dehazing methods) uses a different statistical measure to drive the estimation process(depths estimation), they all share a common shortcoming: when the appearance information of a pixel is unreliable, the algorithms are unable to produce a good depth estimate for the corresponding location in the image. " [19]. The first assumption is, that neighbouring pixels have similar depths, which really isn't new to dehazing methods, but is used in most methods. However, the new assumption is, that for outdoor surveillance cameras, a geometry like in figure 3.9(a) can be assumed. Or in words, the geometry of a camera located above the ground, high in the air and tilted towards the ground. The resulting simple relationship is, that objects which appear closer to the top of the image are usually further away, see figure 3.9(b).

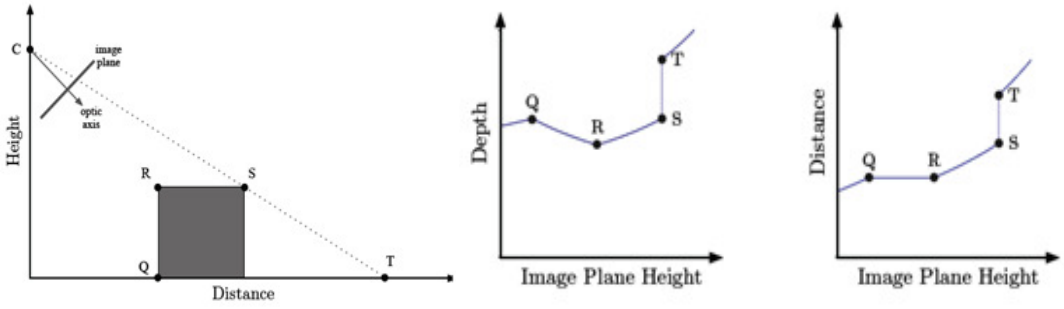

(a) (b) (c)

Figure 3.9.: Assumed camera geometry, the depth of any scene point — i.e., the distance from the centre of projection C - can be split into distance and height components. If the scene does not contain any cave-like surfaces, the distance of scene points will increase monotonically from the bottom of the image to the top,[19]

As the described dehazing methods are using regularisation and optimisation methods, so does this method. Here the graph-cut based α-expansion method is used, as employed by [10]. The assumptions of the geometry are herein used as a preference rather than a hard

constraint and can be used within an energy minimisation framework such as used by [2]. With this as only a soft constraint it even allows for the, in outdoor surveillance unusual, cases in which objects in the top of the image are closer than they should be according to the assumptions. With a static camera position, the depth map can be calculated once and used for several frames in which the atmospheric properties remain roughly the same. A motivation is given by the authors of this method: "The transportation industry would benefit from automatic fog enhancement technology. For this application, the primary interest is enhancing video - not single images." [19]. They also state, that they could perform real-time image dehazing using gpu's(graphics processing units). For this thesis, these are important statements, since a simplification was introduced for static cameras and also a validation that real-time dehazing is in fact possible, however using the GPU rather than a CPU. It can be learned even more from the experiences of Carr and Hartley: "If the camera is positioned high in the air, the difference in depth between a foreground object and the background behind it is usually small. Therefore, one can typically estimate the depth of the background image and apply this to any video frame without creating significant errors in the enhanced image." This principle will be used in the successive section for the development of the real-time dehazer.

However, the error being small, may be greater when estimating the depth map with too much foreground in the scene, such as moving objects occluding parts of otherwise distant surfaces. This would cause an under estimate for those spots in the scene when the background becomes visible again. Due to moving foreground objects it may be convenient to renew the depth map every certain number of frames or when alterations in the scene have been detected by a movement detection algorithm for example. The consequences of using the monotonic depth assumptions compared to an unconstrained method is illustrated in figure 3.10, here the authors Carr and Hartley used a surveillance camera video as input and used the dark channel prior method to enhance the frames in combination with their depth map optimisation method.

As a side note, Carr and Hartley used a gamma correction before applying their dehazing algorithm to the image, as described in an earlier section, which improved the overall contrast, making the work of the dehazer more effective.

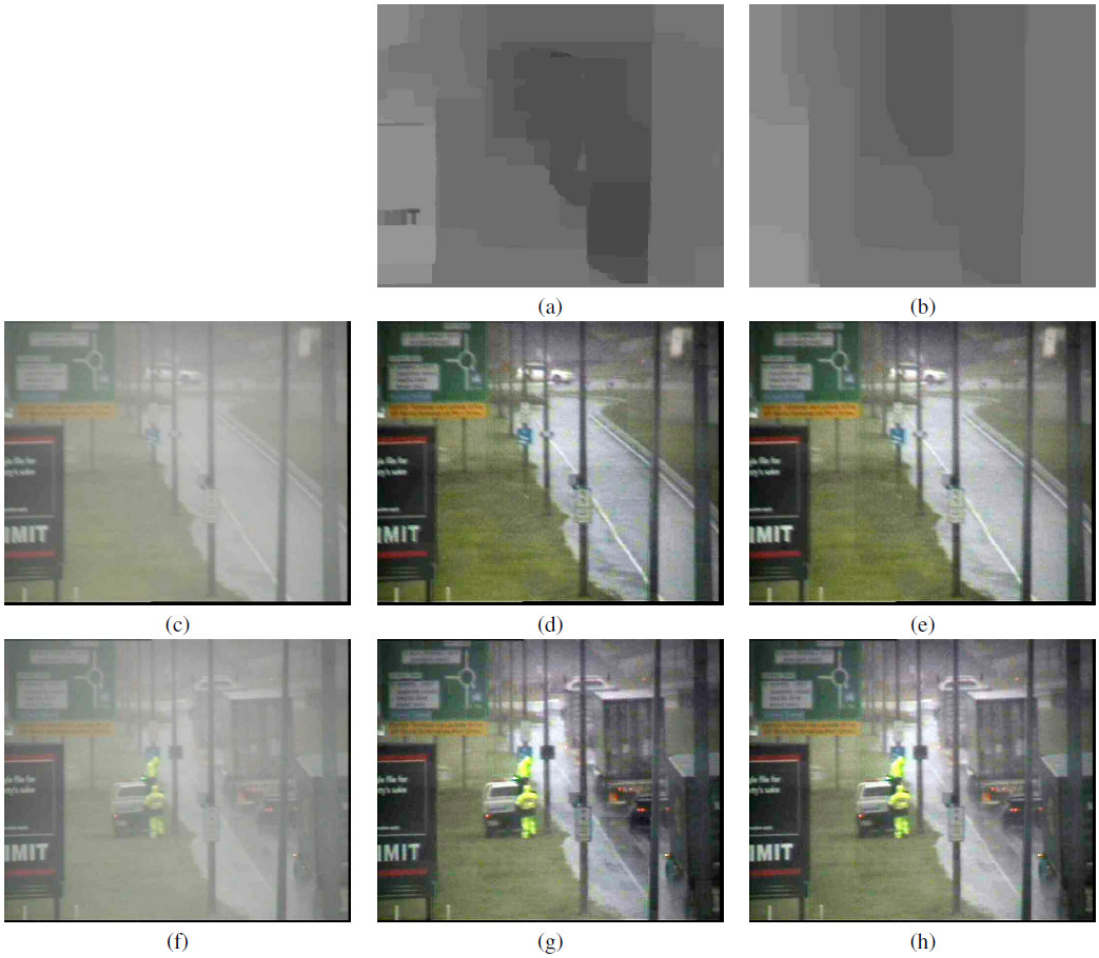

Figure 3.10.: Video frames (c) and (f) are enhanced using depth maps (a) and (b) which were estimated without and with monotonicity respectively. Both depth maps were estimated using the contrast data model applied to video frame (c), as the dark channel prior has difficulty with roads. The unconstrained depth map (a) has outliers (due to the appearance of foreground objects and an inherent difficulty with the textureless road), but these do not induce significant artifacts in the enhancement (d). Since the artifacts are not significant, the improvement in the enhancement (e) from using a monotonic depth map (b) is not substantial. However, when the depth map is applied to a video frame (f) captured later, the outliers in (a) overenhanced the middle vehicle beyond the dynamic range of the image (g). This does not happen in the monotonic correction (h). Although these artifacts may be subtle in image, they are quite apparent in video. [19]

CHAPTER 4

IMPROVED DEHAZING METHOD

Here we describe the dehazing algorithm developed for this thesis. Quoting Namer: "This work is thus a part of process of making the method more useful and reliable ." [1], talking about the image dehazing and polarisation based dehazing in particular. So is this work, dehazing methods came a long way from Koschmieder's theory and the development of fast computer technology along with electronic video sensors.

For this thesis a dehazing algorithm was implemented with new improvements that transmission map was refined using opening (erosion and dilation) of it. In this chapter, the choice of the algorithm basis is explained. In the next step, the working principle of this implementation with a description of the improvements is given and the problem of bluish distant objects (objects near the horizon appears bluish) have been solved, followed by a section presenting the parameters of the algorithm. The chapter has been rounded off by a section about possible further directions of research.

4.1. Choosing the Algorithm

Here we have chosen a method which Dark- Channel Prior method, which allows a high degree of improved results, is straight forward, logical, works with most scenarios, not just special cases like only certain scene geometries and also works on grey scale images, which is relevant to real world applications. Our algorithm is quite faster than the method proposed by He et al. [24]. We have eliminated the soft matting step and refined the transmission by opening it.

It is also important that the required user interaction is minimal, unlike for example [20]. As we have already seen that He et al.'s method as good as other methods in direct comparison with other dehazing methods in terms of image quality and degree of dehazing or defogging, respectively. Other researchers also chose He et al.'s algorithm as basis for their implementation for a image dehazing method.

4.2. Improved Dark-Channel Prior Implementation

The implementation follows in general the flow process of He et al.'s algorithm, which can be seen in figure 4.1.

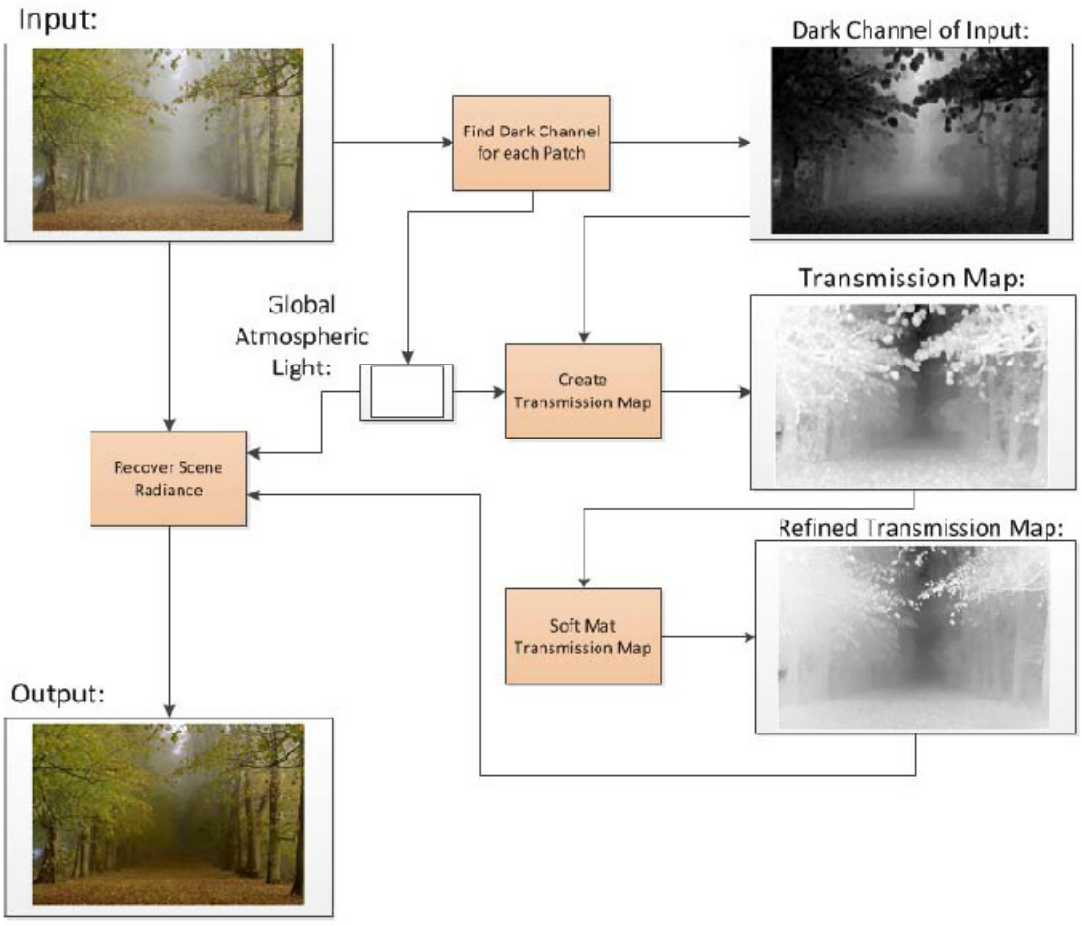

Figure 4.1.: Process flow chart of He et al.'s dehazing method. The patchsize in this example is set to 15x15. The example image is taken from [2]

A component wise analysis of He et al.'s method shows that the processing time predominantly depends on the soft matting algorithm, therefore reducing or even eliminating the processing time of the soft processing would improve the overall dehazing time greatly. More than any attempt is to reduce calculation time in one of the other components. The main idea behind the speed improvement is to eliminate the soft matting step of the transmission map, it is based on the assumption that: "Typically, errors in a depth map do not induce significant artifacts into the enhanced image, since the solution is applied to the data used during estimation." In order to achieve satisfying results, instead

of using soft matting, we have used opening of the transmission map for refining it.This way blocky and halo artifacts are reduced when leaving out the soft matting step. Chengming Zou and Jinrui Chen [21] proposed a method to refine the dehazed image by dilating and eroding it, thus refining block effect and halo effect. However this method leads to blurring of images and details are reduced.

We introduce an improved single image dehazing method, in which we refine the transmission map by Opening (eroding and dilating) it, we use this refined transmission map for generating the dehazed image thus reducing block and halo artifacts, while preserving the details. Compared to [21] this method can obtain better results.

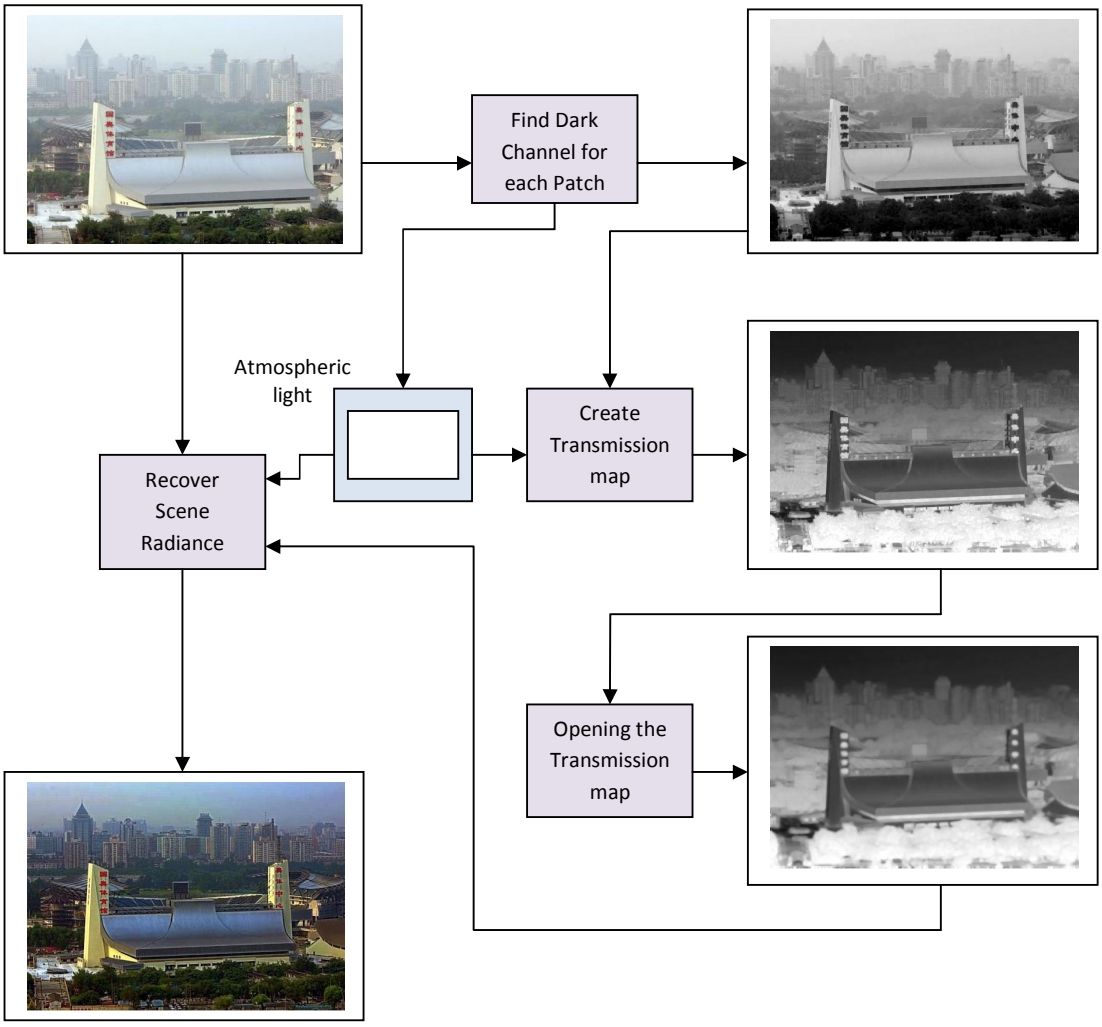

Figure 4.2.: Process flow chart of the dehazing method. The patchsize in this example is set to 4x4.

4.2.1 Dark Channel Prior

The concept of dark channel prior is based on our observation of outdoor haze-free images. As per the prior, in most of the local regions in haze- free images that aren't sky, very often some pixels in at least one of its colour channels(RGB) have very low intensity or close to zero. The dark channel J^{dark} of J(the haze-free image) is defined as (Fig. 4.3):

$$J^{dark}(x) = \min_{c\epsilon\{r,g,b\}} \left(\min_{y\epsilon\Omega(x)} \left(J(y) \right) \right) \tag{4.1}$$

where J^c is a colour channel of J and $\Omega(x)$ is a local patch centered at x. This statistical observation is called the *dark channel prior*:

$$J^{dark}(x) \to 0 \tag{4.2}$$

Figure 4.3.: Haze-free images (top) and their corresponding dark channel (below)

The low intensity in the dark channel is mainly due to three factors: a) shadows, e.g., the shadows of cars, buildings, and the inside of windows in cityscape images, or the shadows of leaves, trees, and rocks in landscape images; b) colorful objects or surfaces, e.g., any object with low reflectance in any color channel (for example, green grass/tree/plant, red or yellow flower/leaf, and blue water surface) will result in low values in the dark channel; c) dark objects or surfaces, e.g., dark tree trunks and stones. As the natural outdoor images are usually colorful and full of shadows, the dark channels of these images are really dark!

4.2.2 Estimating the Atmospheric Light

In most of the previous works, the color of the most haze-opaque region is used as atmospheric light **A** [10] or as **A**'s initial guess [23]. However, little attention has been paid to the detection of the "most haze-opaque" region.

Tan [10] has assumed that the atmospheric light (**A**) is globally constant. Thus the global value can be obtained from the pixels that have the highest intensity in the input image. This is true only when the weather is overcast and the sunlight can be ignored. In this case, the atmospheric light is the only illumination source of the scene.

Unlike other workers in the field, He et al. [24] do not take the pixel with the highest intensity as the atmospheric light, since this could as well be a white surface such as a white airplane or a bright building very near. He used the dark channel to detect the most haze-opaque region and improve the atmospheric light estimation. Here it is assumed that when the pixels are at infinite distance($t \approx 0$), the brightest **I** is the most haze-opaque and it approximately equals **A**.

He et al. pick the top 0.1% brightest pixels in the dark channel ($\min_c(I_c)$), since these must be the most haze-opaque. Among these pixels, the pixel with the highest intensity in the input **I** is picked as the atmospheric light **A**. This may not be the brightest pixel in the image, but is more robust than the "brightest pixel" method according to He et al. [24].

4.2.3 Estimating the Transmission

For estimating the transmission, we can use the atmospheric light **A** from section 4.2.2. Here it is assumed that the transmission in the local patch $\boldsymbol{\Omega(x)}$ is constant. The dark channel J^{dark} of J(the haze-free image) is defined by the equation (4.1), and since J^{dark} tends to be zero and as A^c, the corresponding channel of the atmospheric light is always positive, it may be written:

$$J^{dark}(x) = \min_{c\epsilon\{r,g,b\}} \left(\min_{y\epsilon\Omega(x)} \left(\frac{J^c(y)}{A^c} \right) \right) = 0 \tag{4.3}$$

where J^c is a colour channel of J and $\Omega(x)$ is a local patch centered at x. This can be used to estimate the transmission for that patch $\Omega(x)$ by using equation (4.3) into the image formation model equation (3.12), however now in combination with the min operator:

$$\min_{c}\left(\min_{y\epsilon\Omega(x)} I^{c}(y)\right) = t(x)\min_{c\epsilon\{r,g,b\}}\left(\min_{y\epsilon\Omega(x)}\left(J(y)\right)\right) + \left(1 - t(x)\right).A^{c} \tag{4.4}$$

with $t(x)$ denoting the transmission in a local patch, and as $J^{dark}(x) \to 0$, equation (4.4) leads to:

$$t(x) = 1 - \min_{c\epsilon\{r,g,b\}}\left(\min_{y\epsilon\Omega(x)}\left(\frac{I^{c}(y)}{A^{c}}\right)\right) \tag{4.5}$$

which is a direct estimation of the transmission for each local patch. As we know that dark channel prior is not a good prior for the sky regions, but fortunately, the color of the sky in a hazy image **I** is usually very similar to the atmospheric light **A**. So, in the sky region, we have

$$\min_{c\epsilon\{r,g,b\}}\left(\min_{y\epsilon\Omega(x)}\left(\frac{I^{c}(y)}{A^{c}}\right)\right) = 1 \; and \; thus \; t(x) \to 0 \tag{4.6}$$

Since the sky is at infinite and tends to has zero transmission, the equation (4.5) gracefully handles both sky regions and non-sky regions. We do not need to separate the sky regions beforehand.

As we know that even on clear days the atmosphere is not absolutely free of any particle. There always exist some haze when we look at distant objects. Moreover, the presence of haze is a fundamental cue for human to perceive depth. This phenomenon is called aerial perspective. If the haze is thoroughly removed, the image may seem unnatural and we may lose the feeling of depth. So, we can optionally keep a very small amount of haze for the distant objects so that image seems natural, by introducing a constant parameter ω ($0<\omega\leq1$) into equation (4.5):

$$t(x) = 1 - \omega\min_{c\epsilon\{r,g,b\}}\left(\min_{y\epsilon\Omega(x)}\left(\frac{I^{c}(y)}{A^{c}}\right)\right) \tag{4.7}$$

Therefore we adaptively keep more haze for the distant objects. The value of ω is application based. As we know that the recovered scene radiance is oversaturated for a small patch size, thus as we decrease the patch size we can use slight lower value for ω (≈0.8) and for large patch size we can increase the ω value. We fix it to 0.95 for all results reported in this thesis.

The main problems with the transmission maps are that they suffer from some halos and block artifacts. This is because the transmission is not always constant in a patch. In the next section, we propose a method to refine the transmission maps.

4.2.4 Opening the Transmission map

We refine the transmission map by opening it. Eroding and Dilating [23] are the fundamental operations of morphology, widely used in the image processing. Eroding of **A** by **B** is defined as

$$A \ominus B = \{z|\ (B)_z \cap A^C \neq \phi\} \tag{4.8}$$

where **B** is the structure element. Eroding is to shrink the image in one manner and to some degree controlling by a structure. That **A** is dilated by **B** means that all the original points of **B** construct a new set. After mapped and moved, **B** and part of **B** overlapped. Dilation is defines as

$$A \oplus B = \{z|\ B_z \cap A^C \neq \phi\} \tag{4.9}$$

Opening generally smoothes the contours of the objects in the image, breaks narrow isthmuses, and eliminates thin protrusions. The opening of set **A** by structuring element **B** is defined as

$$A \circ B = (A \ominus B) \oplus B \tag{4.10}$$

Thus opening **A** by **B** is the erosion of **A** by **B**, followed by dilation of the result by **B**. We apply opening by eroding and dilating the transmission map and the structure elements are line and disk respectively.

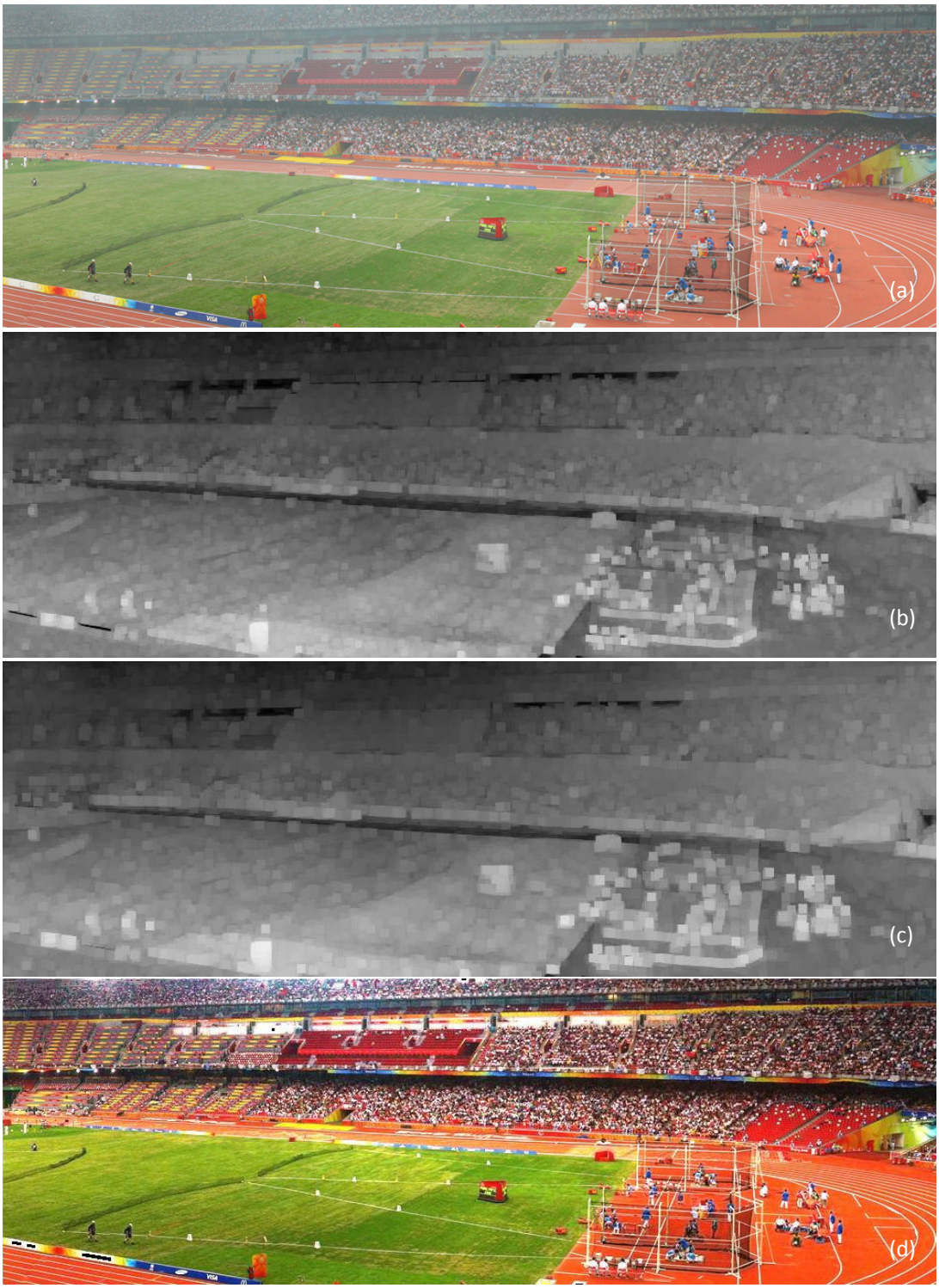

Figure 4.4.: (a) Input image, (b) Transmission map, (c) Opening the Transmission map, (d) Our results.

4.2.5 Recovering the Scene Radiance

Having the transmission map, the scene radiance according to equation (3.12) can be recovered. However, since the direct attenuation term $J(x)t(x)$ can be very close to zero, the transmission is restricted to a lower bound t_0 for example $t_0 = 0.1$, since the scene radiance is typically not as bright as the atmospheric light A. The final scene radiance $J(x)$ may then be recovered by:

$$J(x) = \frac{I(x)-A}{max(t(x),t_0)} + A \tag{4.11}$$

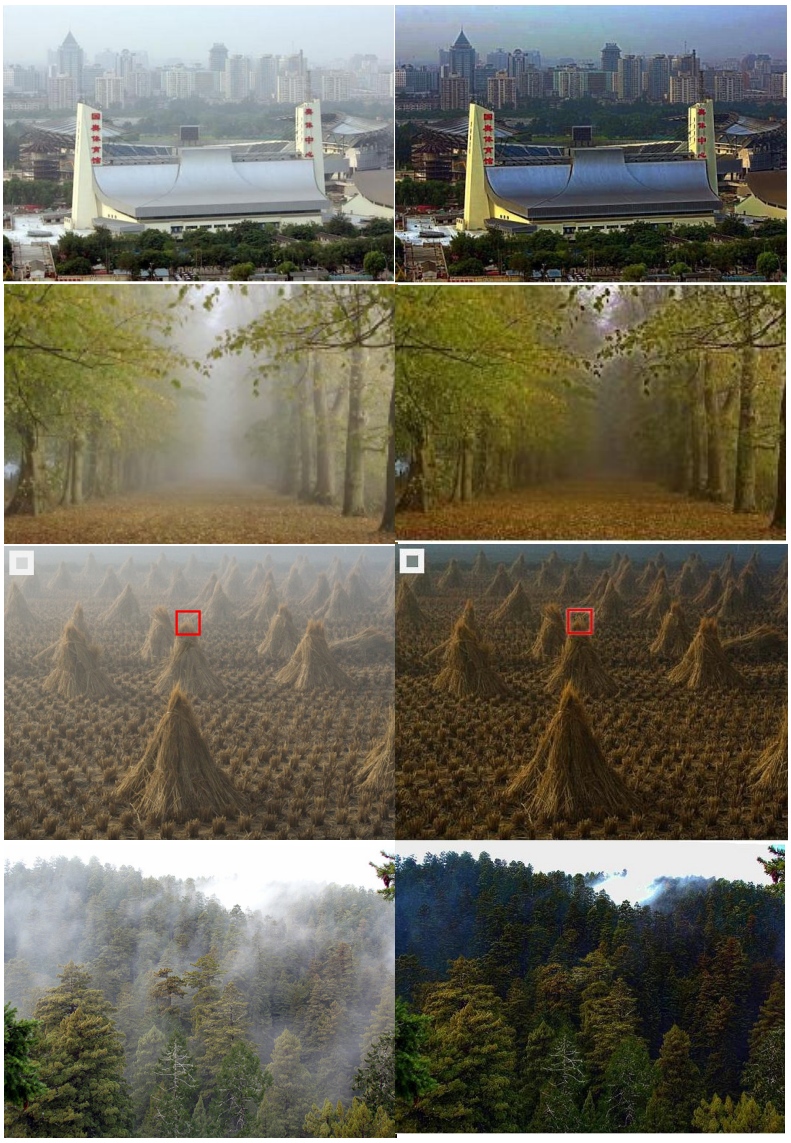

Figure 4.5.: Haze removal results. (a) Input hazy images (left). (b) Restored haze-free images (right)

A typical value of t_0 is 0.1 [24]. Since the scene radiance is usually not as bright as the atmospheric light, the image after haze removal looks dim. So we increase the exposure of J(x) for display. In Figure 4.5 results of our algorithm have been demonstrated.

We have applied our algorithm on videos as well. The input consists of hazed environment and using the algorithm we have dehazed the video. Here we can see few frames of the input video and the dehazed results in Figure 4.6. We have tested our algorithm on images (corresponding to different weather scenarios) and videos, the results are provided in appendix A and B respectively.

(a) Frame 5 (b) Frame 6 (c) Frame 7

(d) Frame 174 (e) Frame 175 (f) Frame 176

Figure 4.6.: Haze removal results. Input video(top frames in each set), output dehazed video(below frames in each set)

4.3 Dehazing of Distant Region

Images taken under bad weather conditions such as fog, mist, rain and snow suffer from poor contrasts and severely corrupted colors. In bad weather, the radiance from a scene point is significantly altered due to atmospheric scattering. The amount of scattering depends on the distances of scene points from the observer. Therefore, restoring clear day contrasts and colors of a scene from a single image taken in bad weather is inherently under-constrained [20]. The transmission *t(x)* is wavelength dependent if the particles in the atmosphere are small (i.e., the haze is thin) and the objects are kilometres away. In this situation, the transmission is different among color channels. This is why the objects near the horizon appear bluish (Fig. 19a). As the haze imaging model (3.12 on page 30) assumes common transmission for all color channels, our above method may fail to recover the true scene radiance of the distant objects and they remain bluish.

Thus we propose a new method to tackle the different transmission among the color channels. Here we estimate the atmospheric light for each color channel independent of the other. The transmission map is estimated for each color channel independent of other and using the respective atmospheric light for that color channel. Therefore the transmission $t_c(x)$ is given by

$$t_c(x) = 1 - \omega \left(\min_{y \epsilon \Omega(x)} \left(\frac{I^c(y)}{A^c} \right) \right) \tag{4.12}$$

where ω is the dehazing parameter. For estimating the radiance we calculate $J_c(x)$ for each color channel using the respective transmission map and atmospheric light for that color channel. Thus $J_c(x)$ is given by

$$J_c(x) = \frac{I^c(x) - A^c}{max(t_c(x), t_0)} A^c \tag{4.13}$$

Radiance for each color is calculated independent of the other color channel. Now radiance for these color channels can be used for generating the dehazed image. The whole method can be explained in Figure 4.7. Here we can see that the bluish problem is removed here. We can set ω as according to the required transmission for the particular channel. For reducing bluish appearance of distant objects we can set value of ω slightly lower (here we lowered it by 0.05) for blue color channel with respect to other channels.

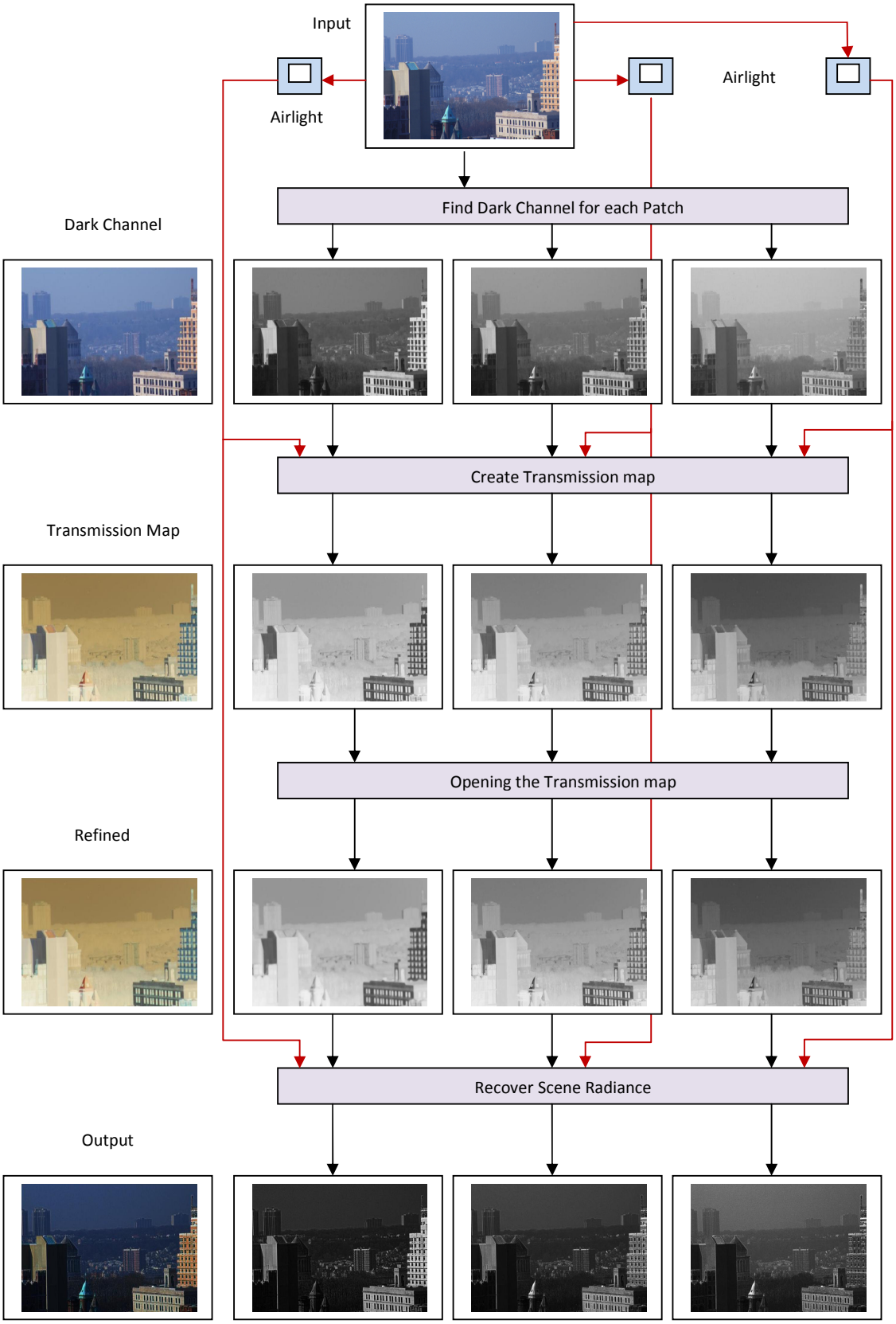

Figure 4.7.: Process flow chart of improved dehazing method. Patchsize is 4x4

Thus we can see that our method can recover the true scene radiance of the distant objects and the objects near the horizon donot appear bluish. In Figure 4.8 we have compared our results with he et al. [24] and we can see that our results are better than he et al.

(a) Input Image (b) Results of He et al. [24]

(c) Transmission map (d) Our results.

(a) Input Image (b) Results of He et al. [24]

(c) Transmission map (d) Our results.

Figure 4.8.: Haze removal results. Comparison with He et al. results.

4.4 Dehazing Parameters

Several parameters can be tweaked in order to achieve satisfying dehazing results. The patchsize of the dark channel and transmission map can be varied. The larger the patchsize is, the more likely it is that the dark channel prior is satisfied, (because the probability that a patch contains a dark pixel is increased and thus the larger the patch size, the darker the dark channel) hence this will assure stronger dehazing. However, larger patches means that the transmission map may be wrong (halos near depth edges may become stronger), since the transmission will not always be constant within a patch. The smaller the patchsize is, the smaller are the visible errors in the dehazed image, especially those along edges but the recovered scene radiance is oversaturated [24]. Figure 4.9 shows the effects of different patchsizes.

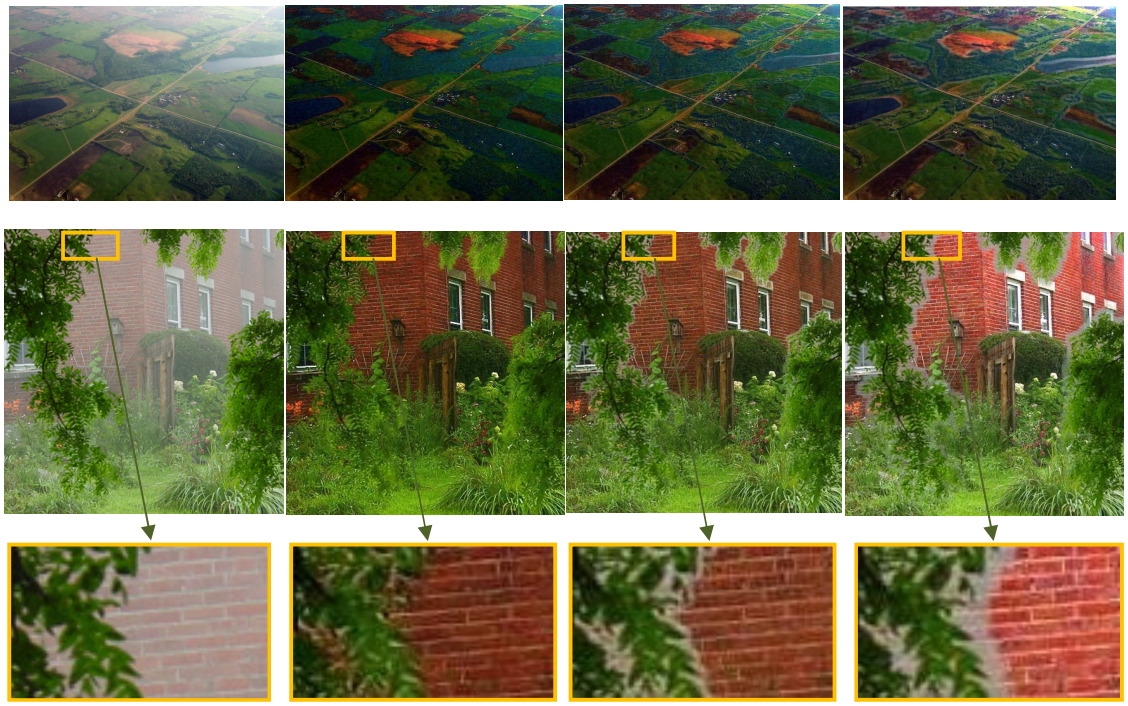

Figure.: 4.9 Recovering images using different patch sizes (after refining). (a) Input hazy images. (b) Using 3 x 3 patches. (c) Using 7x7 patches. (d) Using 15x15 patches.

In Figure 4.9 we can see the haze removal results using different patch sizes. In Figure 3(b), the patch size is 3 x 3. The colors of some surfaces look. In Figures 3(c) and 3(d), the patch sizes are 7 x 7 and 15 x 15, respectively. The results appear more natural than those in Fig. 3(b). This shows that our method works well for sufficiently large patch sizes.

A second parameter stems from equation (4.11). The parameter t_0 defines the lower bound of transmission. When choosing the parameter to be over 100% the application is capable of adding haze to the scene. With t_0 being 0% it has been found in some cases, that artifacts are introduced to the dehazed image due to noise. Also with t_0 = 0%, the sky or other very bright regions are forced to take on a slightly darker colour. Henceforth, choosing a t_0 above zero is also a noise cancelling action. . The effects of alterations to t_0 can be seen in Figure 4.10.

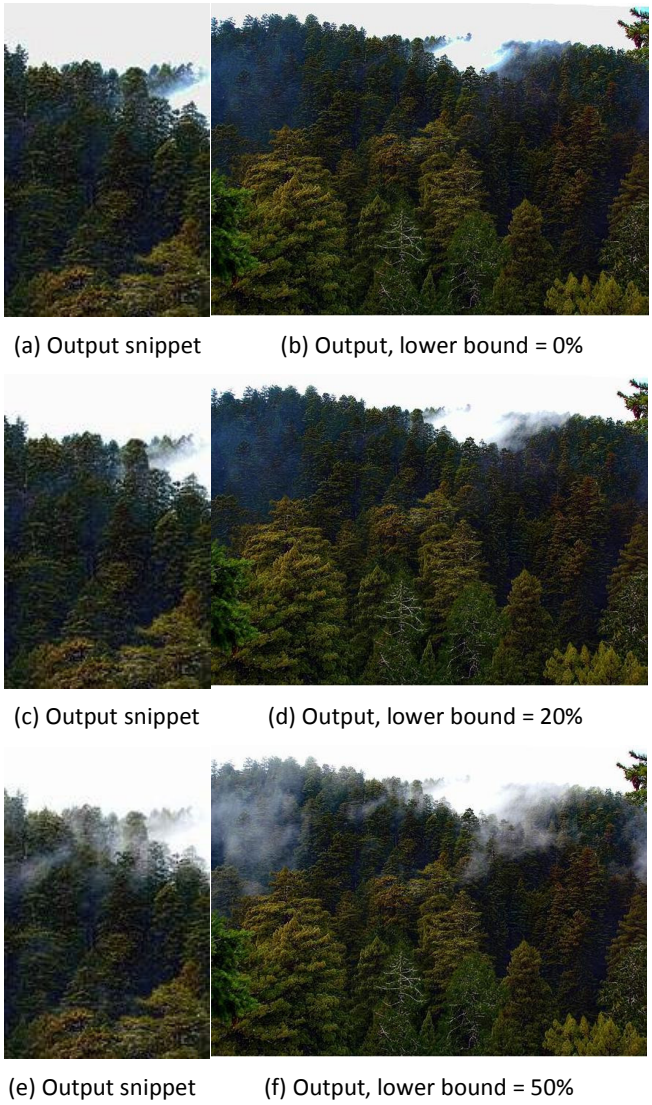

(a) Output snippet (b) Output, lower bound = 0%

(c) Output snippet (d) Output, lower bound = 20%

(e) Output snippet (f) Output, lower bound = 50%

Figure.: 4.10 The effects of increased lower transmission bound

The third parameter regulates the degree of dehazing, He et al.[24] called that parameter ω, which is a real number between zero and one. It assures that more haze is kept at more distant objects. Reason for its introduction is that completely haze free images may seem

unnatural and the feeling of depth may be lost for the viewer due to the effect called *aerial perspective*. Secondly, the physical background of the dark channel prior actually assumes an haze free image, however manages to handle certain degrees of noise well. Since the input image is never free of haze, ω has been found to give reasonable results at about 95% due to testing. The effects of alterations to ω can be seen in Figure 4.11.

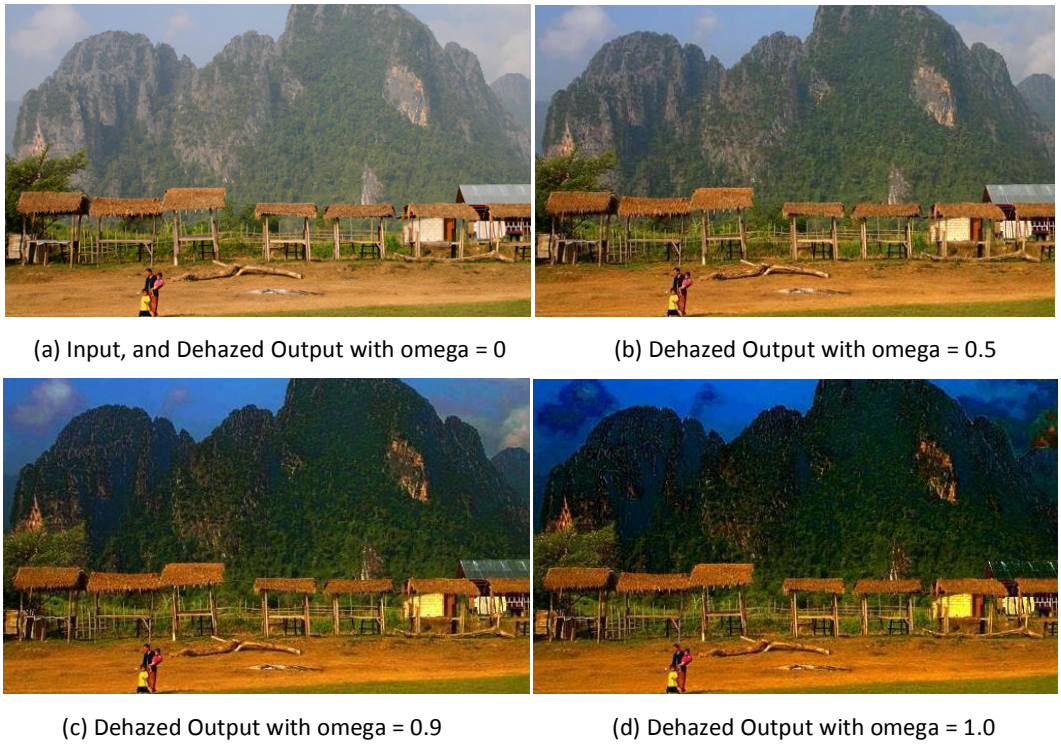

(a) Input, and Dehazed Output with omega = 0

(b) Dehazed Output with omega = 0.5

(c) Dehazed Output with omega = 0.9

(d) Dehazed Output with omega = 1.0

Figure.: 4.11 The effects of decreased ω to the output image.

4.5 Further Research

Visibility in dehazed images have been improved by the implementations like that of He et al. Other versions of implementation, like the one presented here, can perform dehazing fast, meaning, in real-time. However, this method still needs further research and improvements. Due to the eliminated soft matting step in this implementation, image quality is compromised in some cases as it has been shown. It is therefore desirable to find a filter for the transmission map that gives similar results as the soft matting, but can be performed in less time.

Like Kopf et al.'s research, more effort could also go into finding more applications for the depth map of the scene which could be easily attained from the transmission map. As

another example for use, a new application was investigated by Hautière and Aubert [25] who dealt with on board cameras on street vehicles who also performed dehazing/defogging, in this case it is obviously desirable to update the transmission map on every frame since the scene may change significantly on every frame, when at the same time high frame rates are required. Dehazing may also be used as a first image improvement step for other computer vision applications as well, like automatic object detection and tracking. Dehazed images can be used for many applications.

From the theoretical preliminary considerations(section 2.2, page 8) it is known that scattering is affected by wavelength, therefore the transmission depends on the pixel colour and it may be an improvement to generate one transmission map for each colour channel individually, as stated by Lv et al., 2010 [26].

5. Conclusions

In this work, the physical basis for dehazing algorithms has been exhibited and existing methods been described. Today's methods are physically sound and produce qualitatively good results, however for real-time applications they may not always be fast enough. For this thesis a new method was developed on the basis of the dark channel prior, where we refined the transmission map by Opening (eroding and dilating) it.

Bilinear or cross-bilinear filter can be applied further for removing block and halo artifacts but the image gets blurred depending upon the σ_s and σ_r parameters of the bilinear filter. As the haze imaging model assumes common transmission for all color channels, our method may fail to recover the true scene radiance of the distant objects and they remain bluish.

Experimental results show the validity and effectiveness of this method with the help of the test images. For the sake of application orientation, many sets of parameters have been tested by us that are the best usuable for air traffic ground surveillance scenarios. It has been shown in the tests here that although the method was built with just haze in mind, it is possible to even improve foggy, snowy and rainy scenes. Therefore, possible applications are broad, like outdoor surveillance or on board cameras in vehicles [25]. Some researchers even showed that it is possible to improve underwater imaging and aerial photography with similar, if not the same techniques [Schechner and Karpel, 2004b]. Tests in this thesis have confirmed that, like [Kopf et al., 2008] and [He et al., 2010a] stated in their papers, it may be advantageous not to remove the entire haze in the pictures since they may appear unnatural and the observer may lose the awareness of scene depth, since humans rely on haze as an indicator for distance. However, it is certainly dependent on the type of application whether haze should be removed entirely or only to a certain degree.

A. Appendix

TEST ON IMAGES

A.1 Light Haze

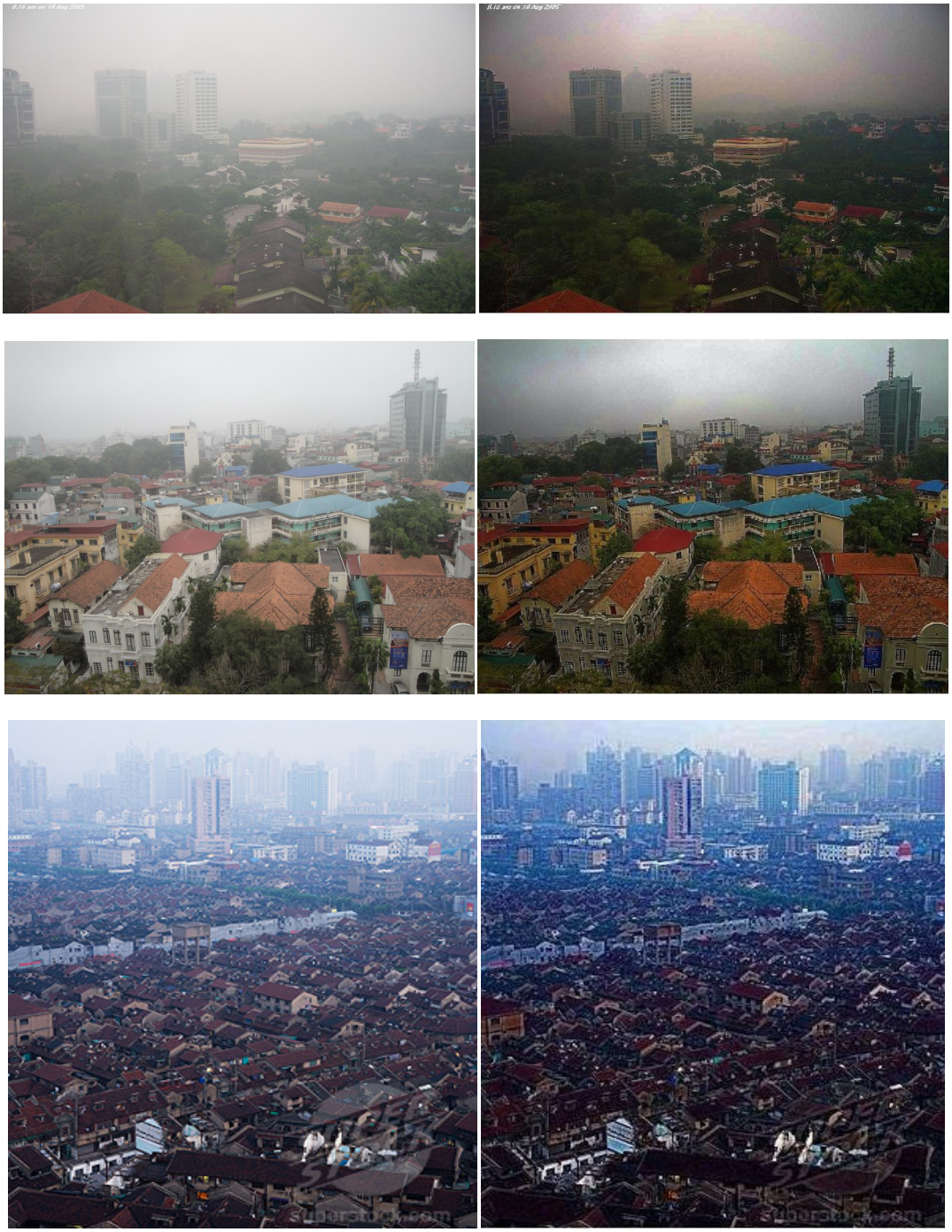

(a) Input Images (b) Our results

A.2 Light Fog

(a) Input Images (b) Our results

A.3 Heavy Fog

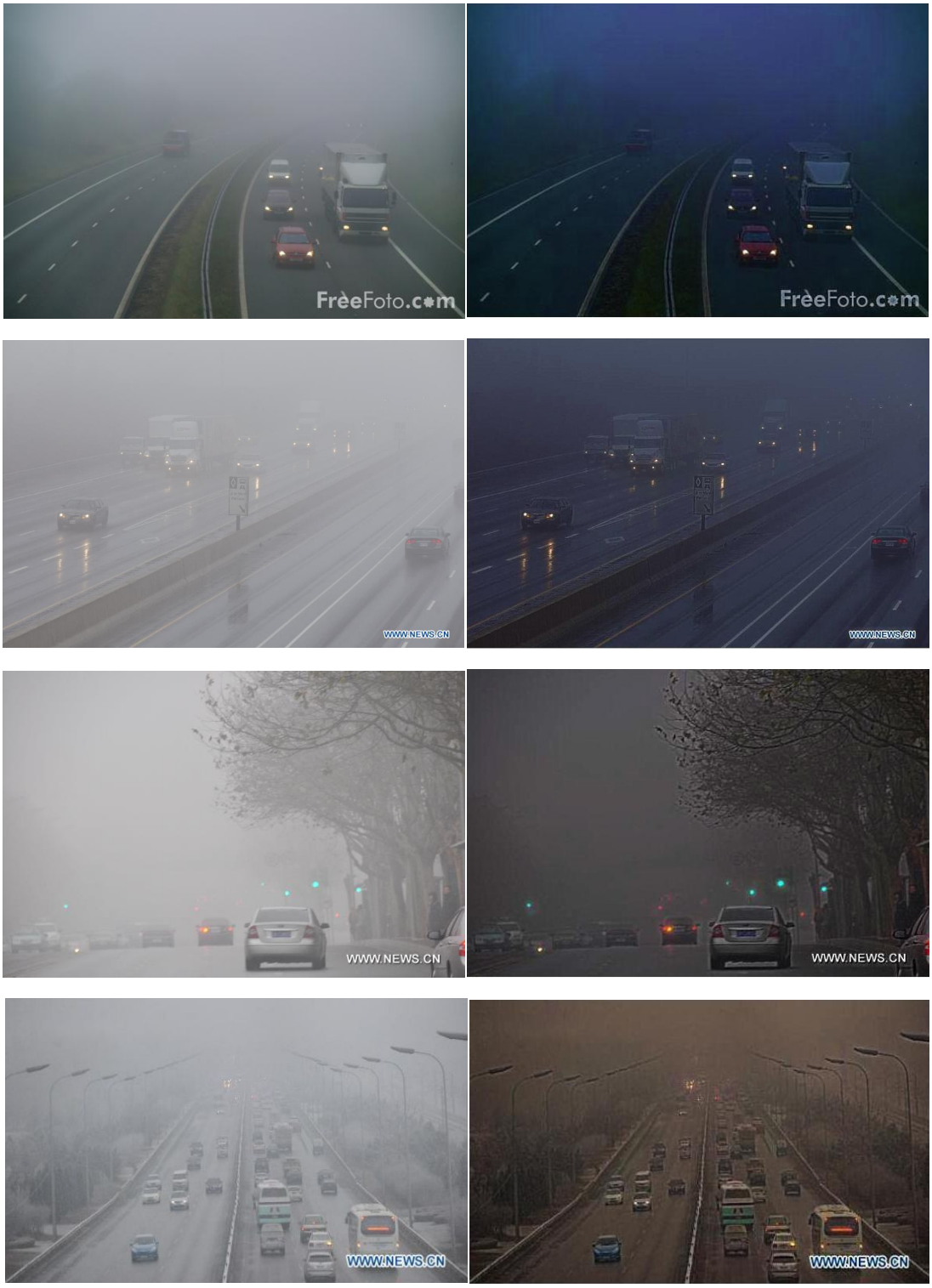

(a) Input Images (b) Our results

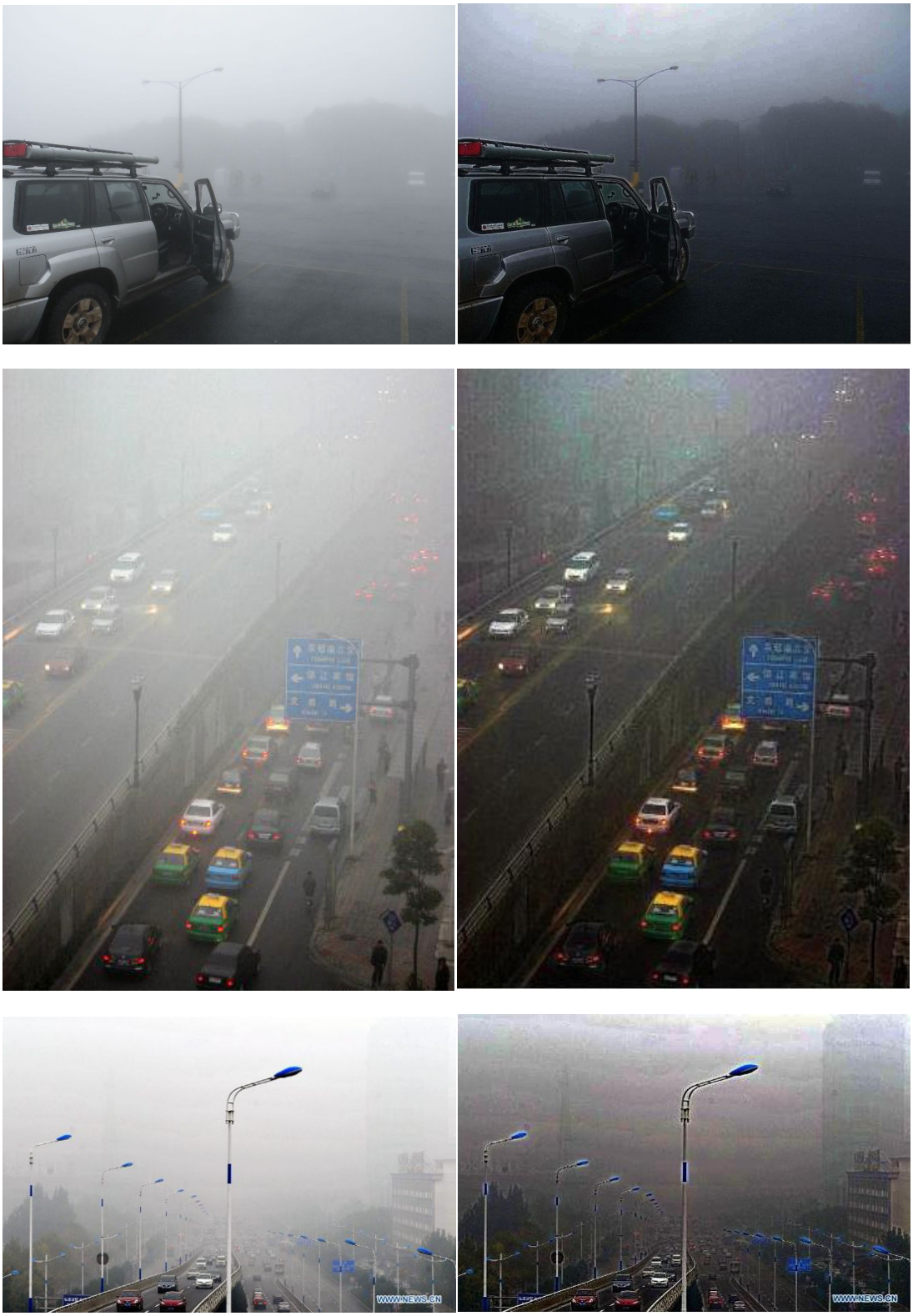

(a) Input Images (b) Our results

A.4 Heavy Rain

(a) Input Images (b) Our results

A.5 Snowstorm

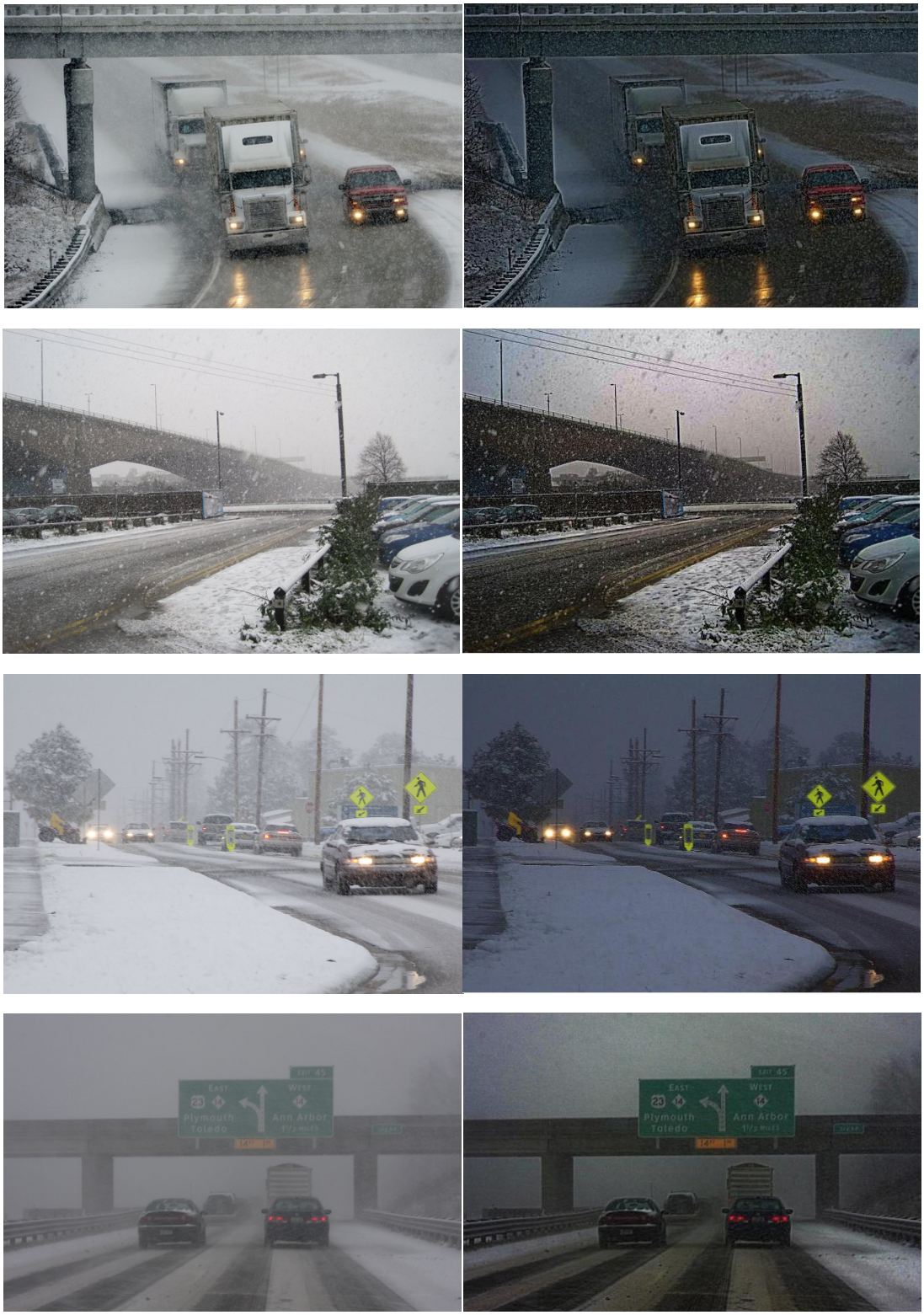

(a) Input Images (b) Our results

B. Appendix

TEST ON VIDEOS

(a) Frame 2 (b) Frame 3 (c) Frame 4

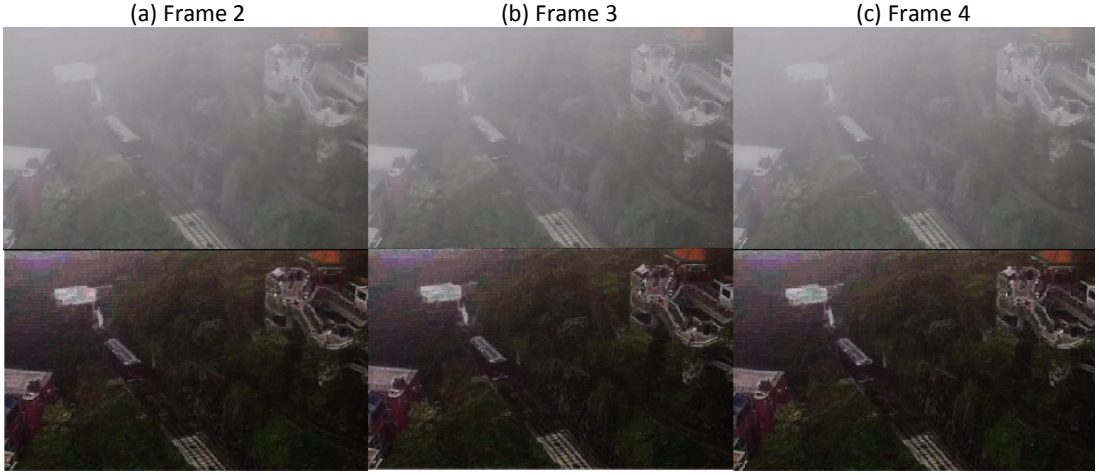

(d) Frame 115 (e) Frame 116 (f) Frame 117

(g) Frame 203 (h) Frame 204 (i) Frame 205

Input video frames (top) and dehazed video frames (below) in each set

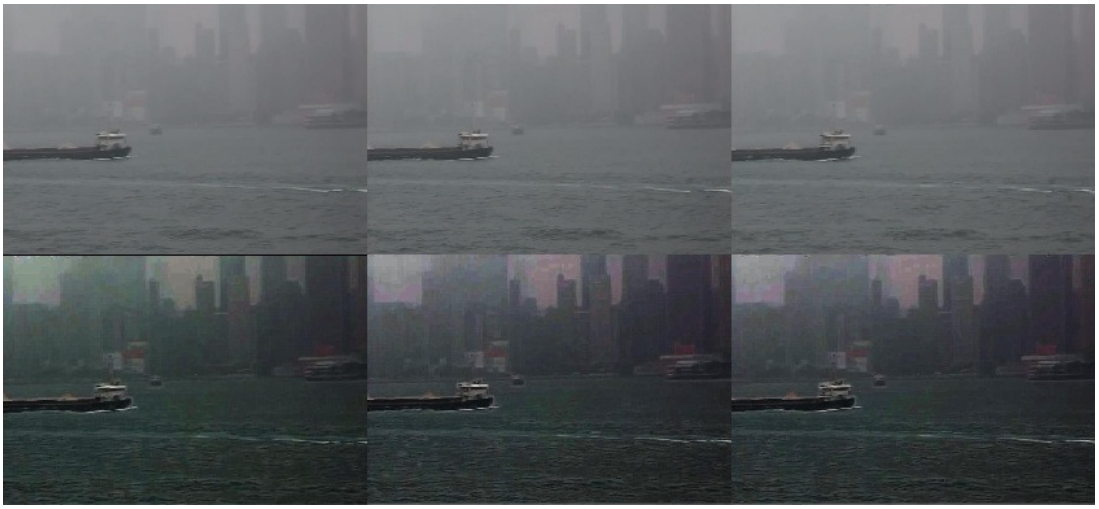

(a) Frame 5 (b) Frame 6 (c) Frame 7

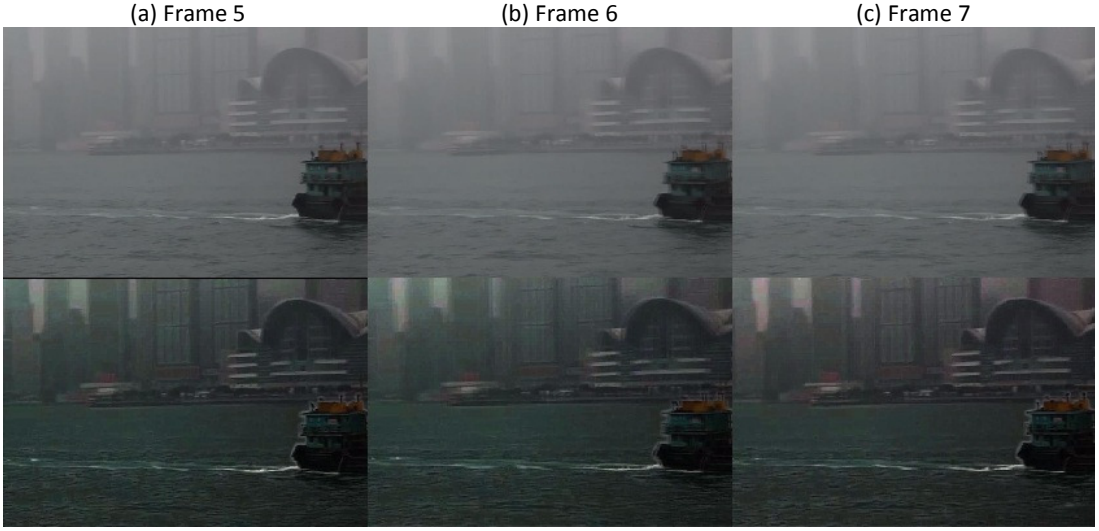

(d) Frame 108 (e) Frame 109 (f) Frame 110

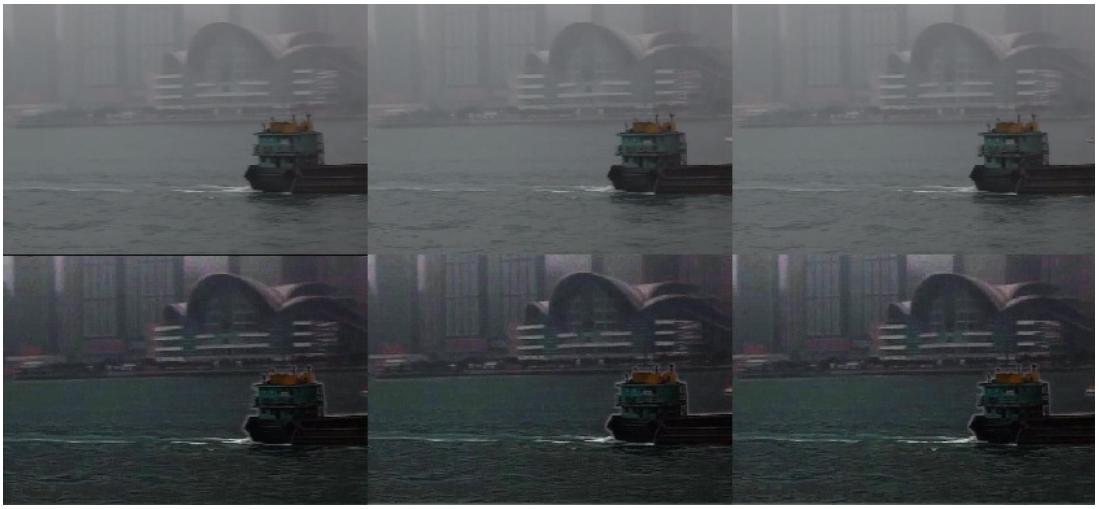

(g) Frame 135 (h) Frame 136 (i) Frame 137

Input video frames (top) and dehazed video frames (below) in each set

Bibliography

[1]. Namer, E. and Schechner, Y. Y. (2005) "Advanced Visibility Improvement Based on Polarizazion Filtered Images."

[2]. He, K., Sun, J. and Tang, X. (2010) "Single Image Haze Removal Using Dark Channel Prior" *Pattern Analysis and Machine Intelligence, IEEE*

[3]. Rayleigh (Lord) (1871) "On the scattering of light by small particles."

[4]. Fattal, R. 2008 *Single Image Dehazing*. SIGGRAPH 2008 #0394

[5]. McCartney, E. J. (1976) *Optics of the Atmosphere.* John Wiley & Sons, New York / London / Sydney / Toronto.

[6]. Dickson D. R. and Hales J. V. (1961) "Computation of Visual Range in Fog and Low Clouds." *Scientific Report for Armed Services Technical Information Agency Virginia.*

[7]. Duntley, S. Q. (1948) "The reduction of apparent contrast by the atmosphere."

[8]. Kopf, J., Neubert, B., Chen, B., Cohen, M., Cohen-Or, D., Deussen, O., Uyttendaele, M., and Lischinski, D. (2008) "Deep photo: Model-based photograph enhancement and viewing." SIGGRAPH Asia 2008

[9]. Schechner, Y. Y., Narasimhan, S. G., and Nayar, S. K. (2001) "Instant dehazing of images using polarization," 325-332.

[10]. Tan, R. T. (2008) "Visibility in bad weather from a single image," *Proceedings of IEEE CVPR*

[11]. He, K., Sun, J. and Tang, X. (2010) "Supplemental Materials" http: //personal.ie.cuhk.edu.hk/~hkm007/cvpr09/.

[12]. cambridgeincolour.com 05-06-2012 19:51 PM http://www.cambridgeincolour.com/tutorials/unsharp-mask.htm.

[13]. Schechner, Y. Y., Narasimhan, S. G., and Nayar, S. K. (2003) "Polarization-based vision through haze," *Optical Society of America,* 20. January 2003, Vol. 42, No. 3, Applied Optics

[14]. Schechner, Y. Y. and Karpel, N. (2004) "Recovering Scenes by Polarization Analysis," Proc. MTS/IEEE Oceans'04, Vol. 3,

[15]. Nayar, S. K. and Narasimhan, S. G. (1999) "Vision in Bad Weather," The Proceedings of the Seventh IEEE International Conference on Computer Vision, September, 1999

[16]. Narasimhan, S. G. and Nayar, S. K "Vision and the Atmosphere," International Journal of Computer Vision

[17]. Rossum, M. V., and Nieuwenhuizen, T. (1999) Multiple scattering of classical waves: microscopy, mesoscopy and diffusion

[18] Shwartz, S., Namer, E. and Schechner, Y.Y. (2006) "Blind Haze Separation," *Computer Vision and Pattern Recognition, 2006 IEEE Computer Society Conference*

[19]. Carr, P. and Hartley, R. (2009) "Improved Single Image Dehazing Using Geometry," *2009 Digital Image Computing: Techniques and Applications,* dicta,

[20]. Narasimhan, S. G. and Nayar, S. K (2003) "Interactive deweathering of an image using physical models," *Workshop on Color and Photometric Methods in Computer Vision*

[21]. Chengming Zou and Jinrui Chen. Recovering Depth from a Single Image Using Dark Channel Prior, ACIS International Conference, 2010

[22]. Yan Wang and Bo Wu. Improved Single Image Dehazing using Dark Channel Prior, 978-1-4244-6585-9/10/$26.00 ©2010 IEEE.

[23]. R.C.Gonzalez. Digital Image Processing Using MATABLE, Prentice Hall Upper Saddle River, New Jersey, 2002.

[24]. Kaiming He, Jian Sun, and Xiaoou Tang. Single Image Haze Removal Using Dark Channel Prior, IEEE TRANSACTIONS ON PATTERN ANALYSIS AND MACHINE INTELLIGENCE, VOL. 33,2011.

[25]. Hautière, N. and Aubert, D. (2005) "Contrast Restoration of Foggy Images through use of an Onboard Camera," *Proceedings of the 8th International IEEE Conference of Intelligent Transportation Systems* Vienna, Austria

[26]. Lv, X., Chen, W., Shen, I. (2010) "Real-Time Dehazing for Image and Video," pacific_graphics, pp.62-69, 2010 18th Pacific Conference on Computer Graphics and Applications.

[27]. Schechner, Y. Y. and Karpel, N. (2004) "Clear Unterwater Vision" Proc. Computer Vision & Pattern Recognition, Vol. I, pp. 536-543

[28]. en.wikipedia.org 02-06-2012 19:16 PM http://en.wikipedia.org/wiki/File:Rayleigh_sunlight_scattering.png.

[29]. en.wikipedia.org 02-06-2012 19:30 PM http://en.wikipedia.org/wiki/File:Gamma06_600.png.

[30]. en.wikipedia.org 02-06-2012 20:15 PM
http://en.wikipedia.org/wiki/File:Histogrammspreizung.png.
[31]. en.wikipedia.org 02-06-2012 20:30
http://en.wikipedia.org/wiki/File:Knysnasunset.jpg

.